Luminosity Evolution of Rotation-Powered Pulsar

HIROTANI, Kouichi

ASIAA/TIARA-NTHU, Taiwan

Fourth International Fermi Symposium
Monterey, CA, USA
October 30, 2012

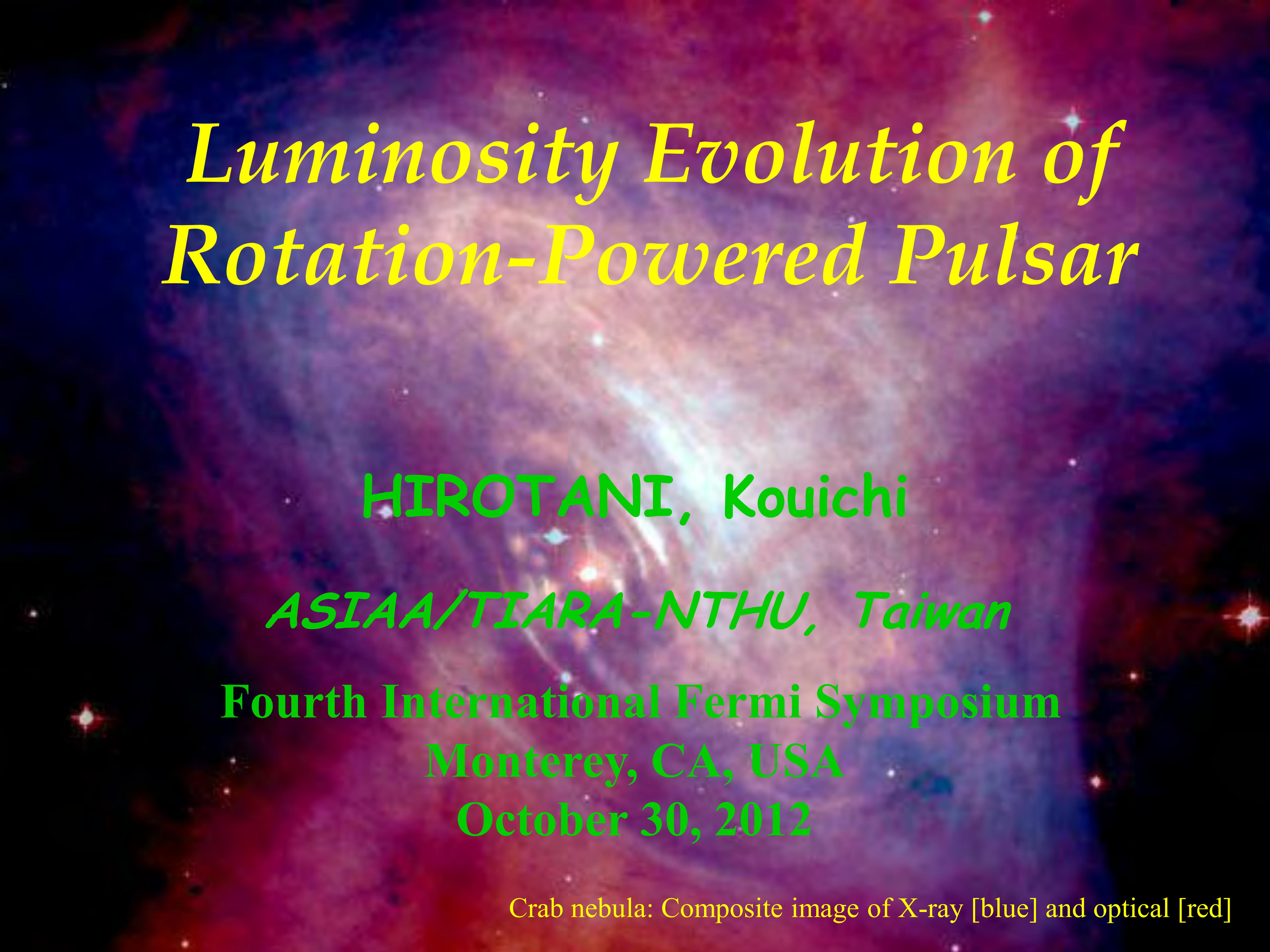

Crab nebula: Composite image of X-ray [blue] and optical [red]

§1 γ-ray Pulsar Observations

After 2008, LAT aboard Fermi has detected more than 100 pulsars above 100 MeV.

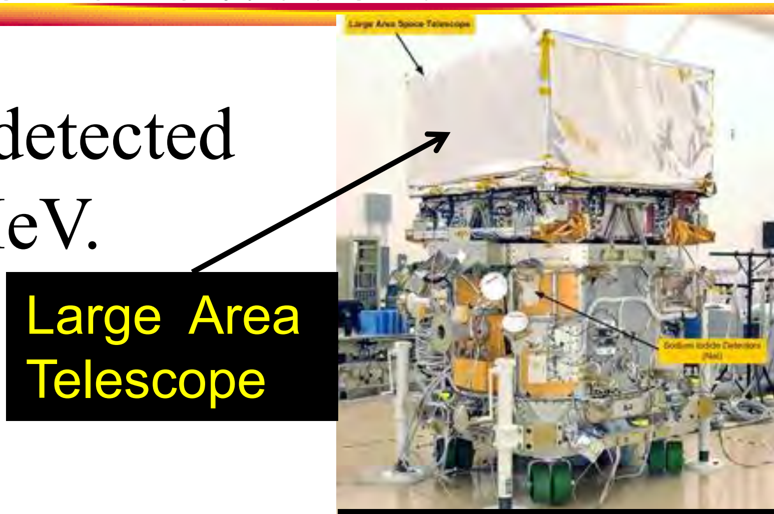

Fermi γ-ray space telescope

Fermi/LAT point sources (>100 MeV)

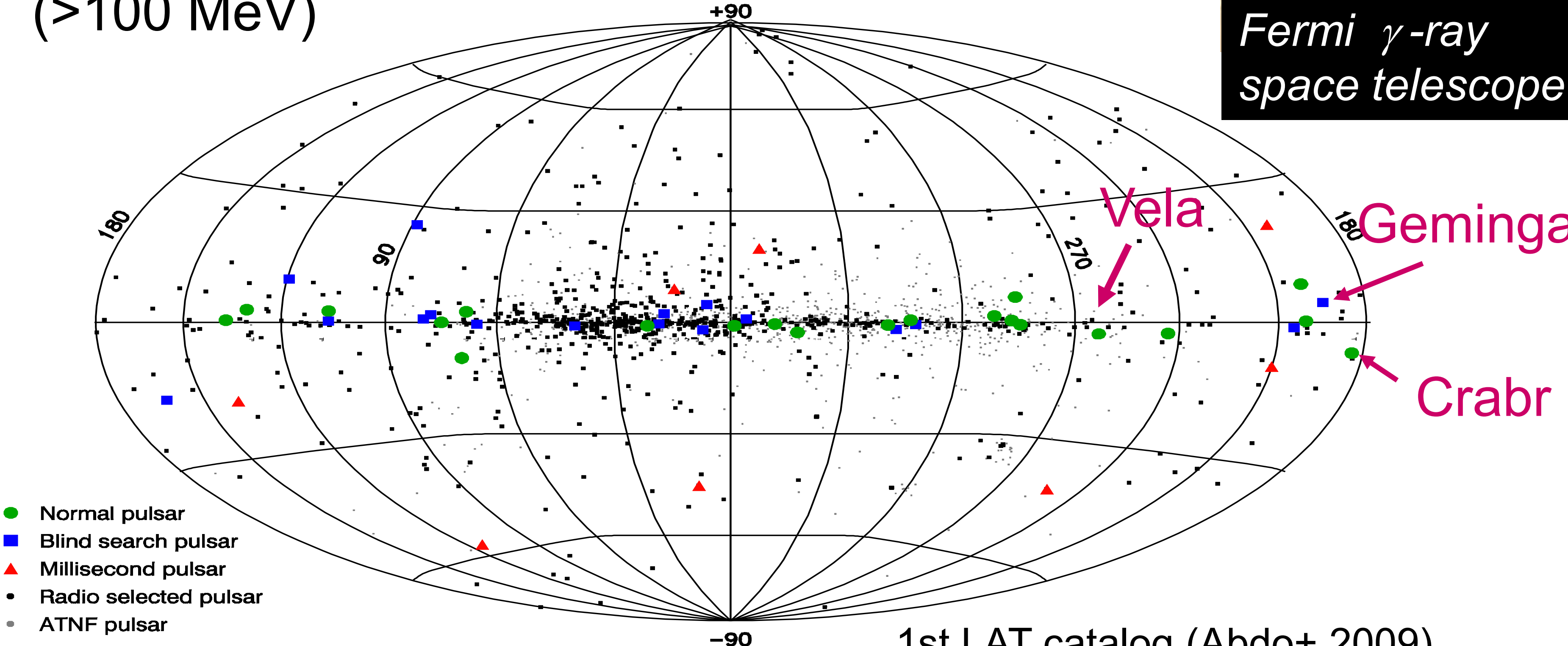

1st LAT catalog (Abdo+ 2009)

Broad-band spectra (pulsed)

- High-energy (>100MeV) photons are emitted mainly via **curvature** process by ultra-relativistic $e^{\pm}$'s.

- Above several GeV, curvature spectrum should show exp. cutoff.

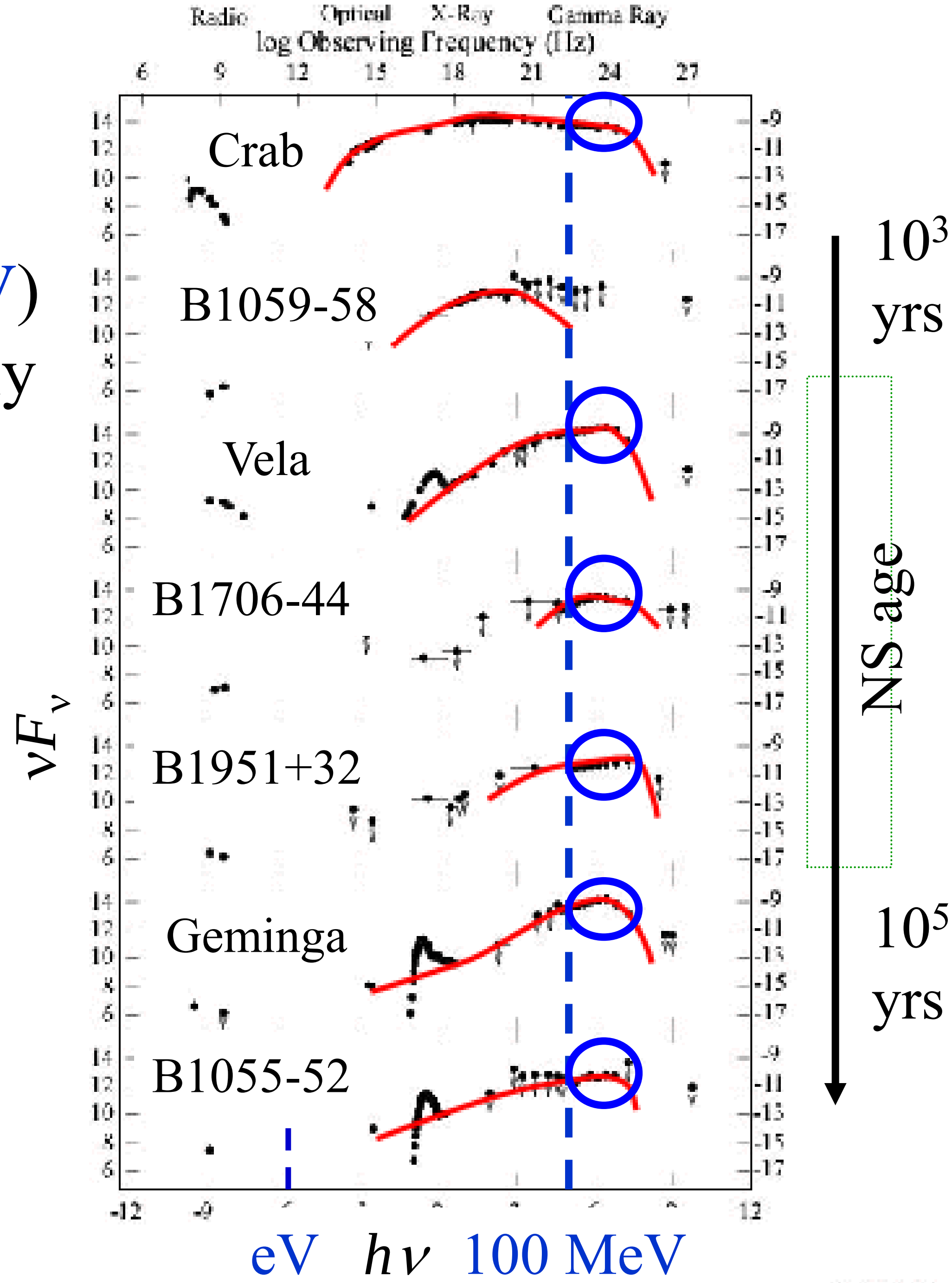

Broad-band spectra (pulsed)

- High-energy (>100MeV) photons are emitted mainly via **curvature** process by ultra-relativistic $e^{\pm}$'s.
- Above several GeV, curvature spectrum should show exp. cutoff.
- However, from the Crab, **ICS by secondary / tertiary pairs** is also observed above 25 GeV.

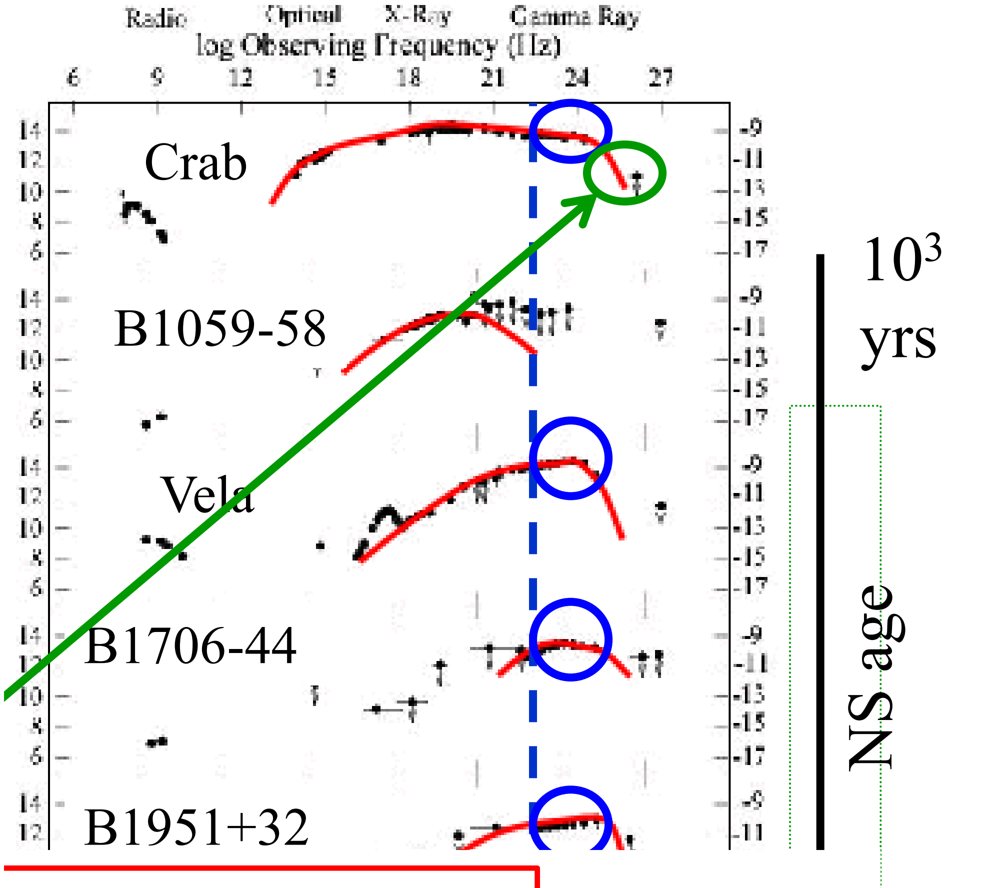

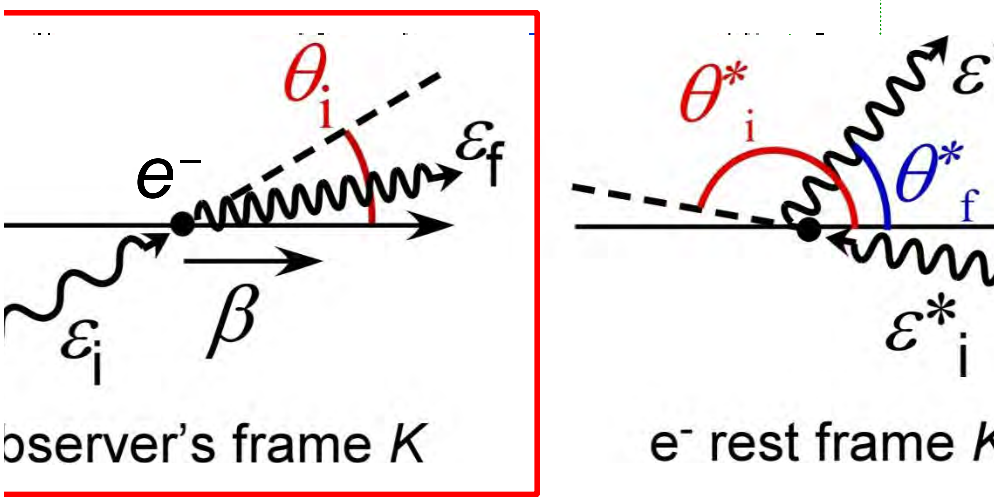

§1 Introduction

Such Crab's sub-TeV component shows that pulsed γ-rays are emitted from the **outer** magnetosphere $(\cancel{\gamma \boldsymbol{B}\rightarrow ee})$.

In addition, **higher-altitude** emission models naturally explain wide-separated double peaks.

We thus consider the outer-gap model (Cheng+ 86, ApJ 300,500) in this talk.

Aleksic + (2012) A&A 540, A69

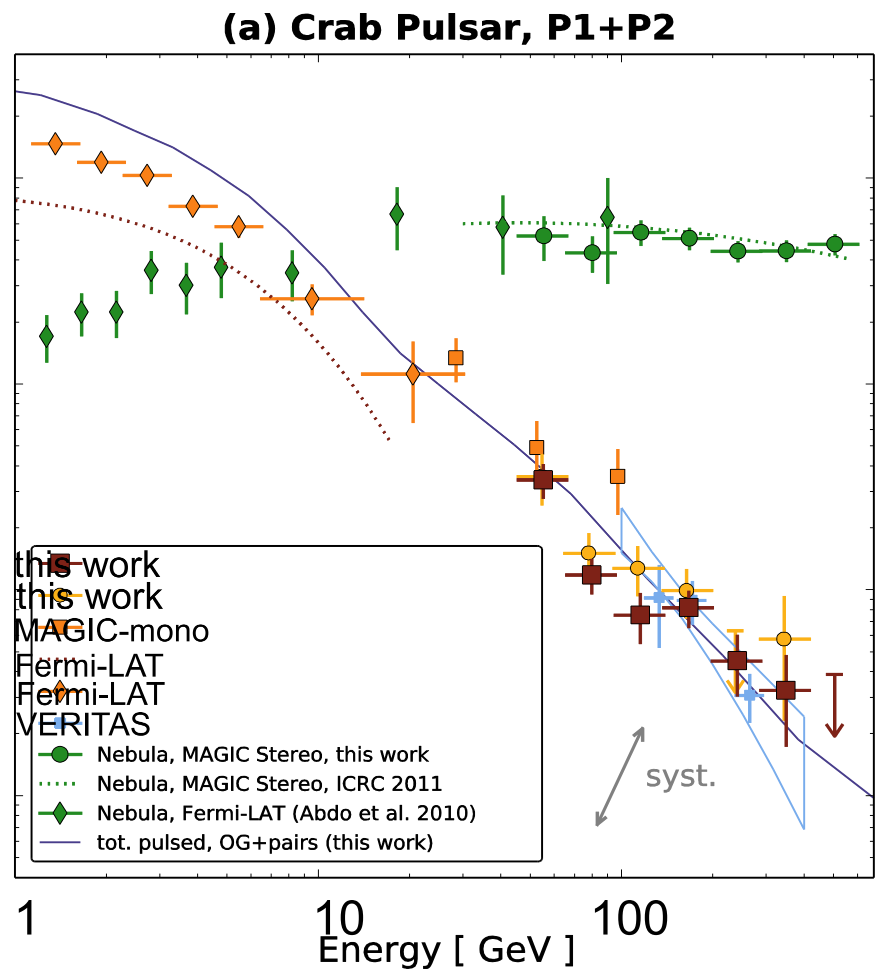

§1 Introduction

Various attempts have been made on recent OG model:

3-D geometrical model

→ phase-resolved spectra (Cheng + '00; Tang + '08)

→ atlas of light curves for PC, OG, SG models (Watters + '08)

2-D self-consistent solution (Takata + '06; KH '06)

3-D self-consistent solution

→ phase-resolved spectra, absolute luminosity if we give only P, dP/dt, α, kT $(+\zeta)$ (this talk)

In this talk, I'll present the most recent results obtained in my 3-D version of self-consistent OG calculations.

§2 *Derivation of* $L\gamma$ *vs.* $L_{\rm spin}$

Today, using the OG mode, we derive the observed relationship, $L_\gamma \propto L_{\rm spin}{}^{0.5}$, both analytically and numerically.

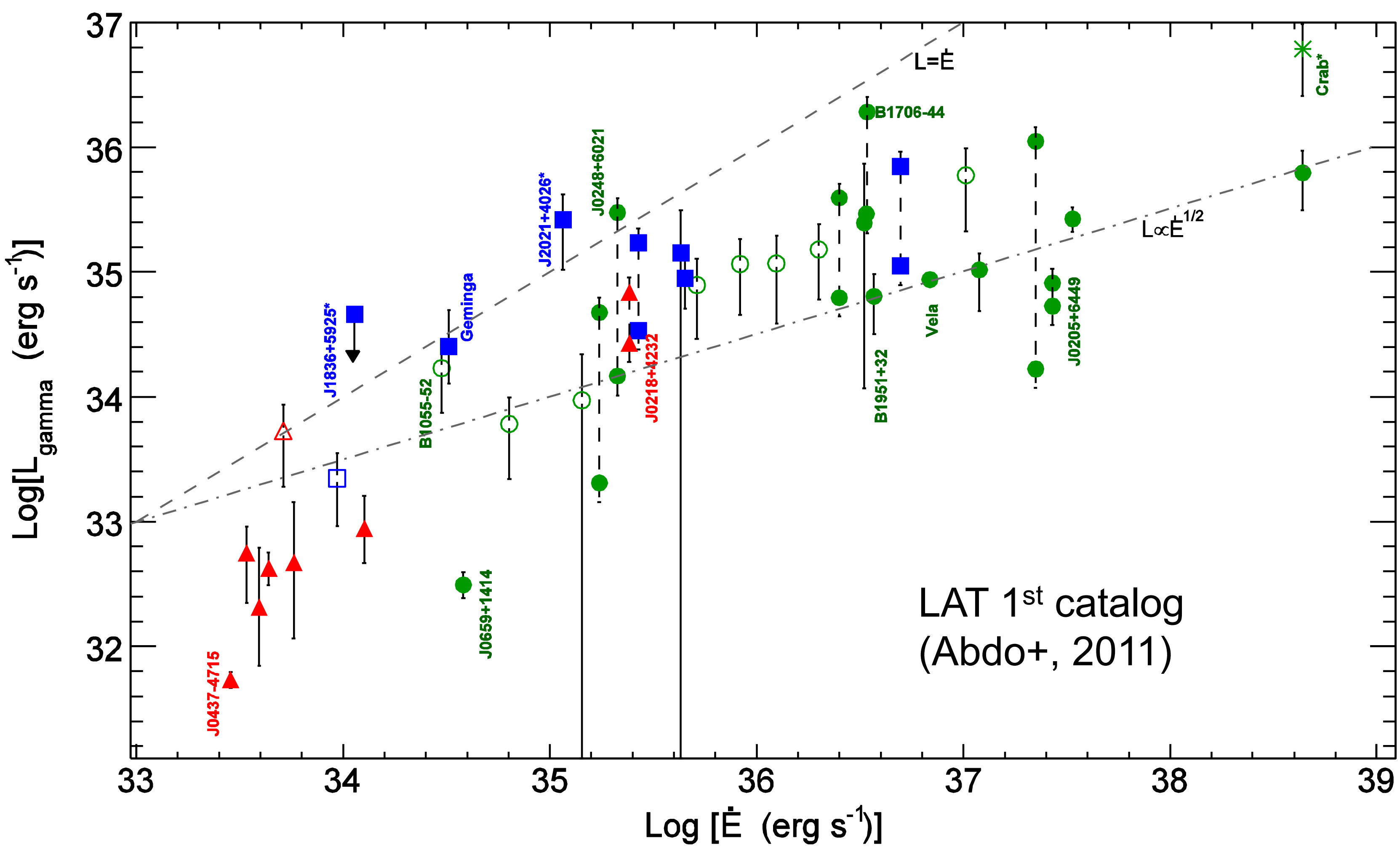

§2 Analytical derivation of L_γ vs. $L_{\rm spin}$

First, **analytically** consider the condition of self-sustained OG. An OG emits the energy flux (KH 2008, ApJ 688, L25)

$$(\nu F_\nu)_{\rm peak} \approx 0.0450 h_{\rm m}{}^3 \frac{\mu^2\Omega^4}{c^3}\frac{1}{d^2},$$

by curvature process, where $h_{\rm m}$ denotes dimensionless OG trans-***B*** thickness, μ the dipole moment, and d the distance.

OG luminosity can be, therefore, evaluated as

$$L_\gamma \approx 2.36(\nu F_\nu)_{\rm peak} \times 4\pi d^2 f_\Omega \approx 1.23 f_\Omega h_{\rm m}{}^3 \underbrace{\frac{\mu^2\Omega^4}{c^3}}_{\propto \dot{E}}.$$

Thus, $h_{\rm m}$ controls the luminosity evolution.

§2 Analytical derivation of $L\gamma$ vs. $L_{\rm spin}$

To examine $h_{\rm m}$, consider the condition of self-sustained OG.

An inward e^- emits $N_\gamma^{\rm in}\sim 10^4$ synchro-curvature photons, $N_\gamma^{\rm in}\tau^{\rm in}\sim 10$ of which materialize as pairs.

Each returned, outward e^+ emits $N_\gamma^{\rm out}\sim 10^5$ curvature photons, $N_\gamma^{\rm out}\tau^{\rm out}\sim 0.1$ of which materialize as pairs.

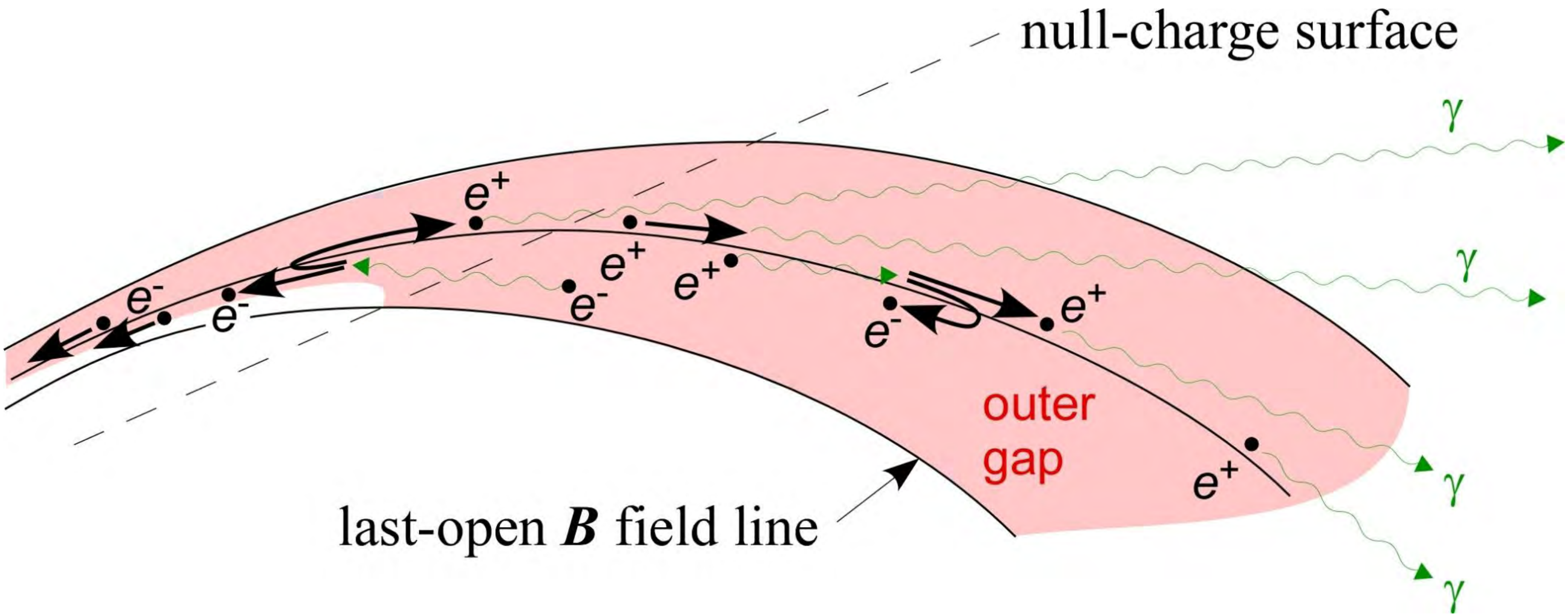

§2 Analytical derivation of $L\gamma$ vs. L_{spin}

To examine h_m, consider the condition of self-sustained OG.

An inward e$^-$ emits $N_\gamma^{in} \sim 10^4$ synchro-curvature photons, $N_\gamma^{in} \tau^{in} \sim 10$ of which materialize as pairs.

Each returned, outward e$^+$ emits $N_\gamma^{out} \sim 10^5$ curvature photons, $N_\gamma^{out} \tau^{out} \sim 0.1$ of which materialize as pairs.

That is, gap trans-***B***-field thickness h_m is automatically regulated so that $N_\gamma^{in} \tau^{in} N_\gamma^{out} \tau^{out} = 1$ is satisfied.

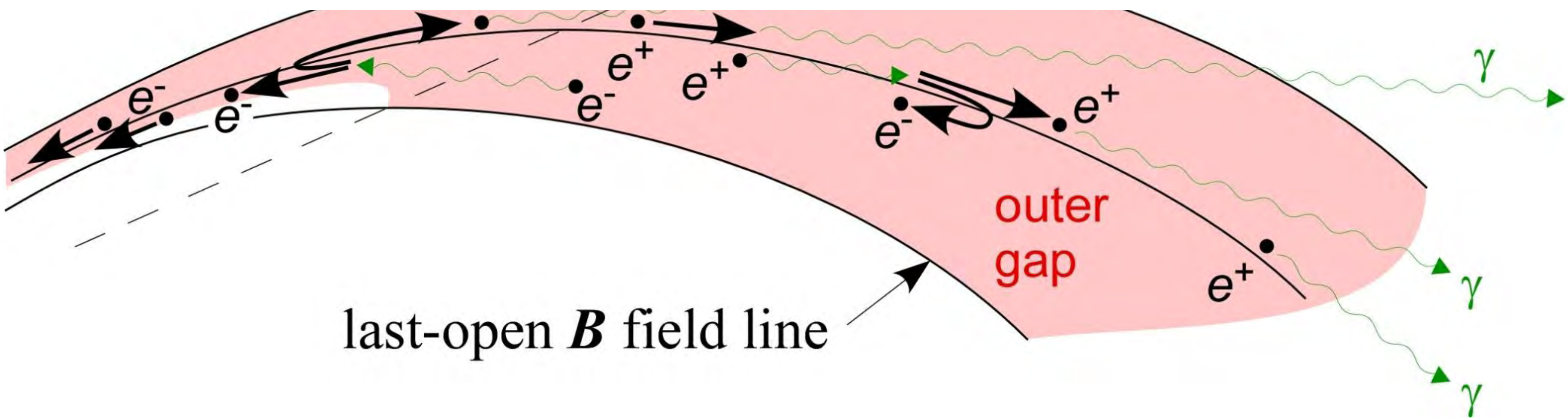

§2 *Analytical derivation of* $L\gamma$ *vs.* L_{spin}

Step 1: Both $N_\gamma^{in}\tau^{in}$ and $N_\gamma^{out}\tau^{out}$ are expressed in terms of P, μ, α, T, and h_m. Thus, $N_\gamma^{in}\tau^{in} N_\gamma^{out}\tau^{out}=1$ gives $h_m = h_m(P, \mu, \alpha, T)$.

Step 2: Specifying the spin-down law, $P=P(t,\alpha)$, and the cooling curve, $T=T(t)$, we can solve $h_m = h_m(t, \alpha)$.

Step 3: On the other hand, $P=P(t,\alpha)$ gives $\dot{E} = \dot{E}(t,\alpha)$.

Step 4: Therefore, we can relate $L_\gamma \propto h_m{}^3 \dot{E}$ and $\dot{E}$ with intermediate parameter, pulsar age, t.

§2 Analytical derivation of L_γ vs. $L_{\rm spin}$

Step 1: express $N_\gamma{}^{\rm in}\tau^{\rm in}$ and $N_\gamma{}^{\rm out}\tau^{\rm out}$ with P, μ, α, kT, $h_{\rm m}$.

OG model predicts

$$E_{||} \approx \frac{\mu}{2\varpi_{\rm LC}{}^3} h_{\rm m}{}^2 .$$

Particles ($e^{\pm}$'s) saturate at Lorentz factor,

$$\gamma = \left(\frac{3\rho_c^2}{2e} E_{||} \right)^{1/4} ,$$

emitting curvature photons with characteristic energy,

$$h\nu_c = \frac{3}{2} \hbar c \frac{\gamma^3}{\rho_c} .$$

§2 Analytical derivation of $L\gamma$ vs. L_{spin}

Step 1: express $N_\gamma^{in}\tau^{in}$ and $N_\gamma^{out}\tau^{out}$ with P, μ, α, T, h_m.

An inward e⁻ or an outward e⁺ emits

$$(N_\gamma)^{in} = eE_{\|} l_2 / h\nu_c, \quad (N_\gamma)^{out} = eE_{\|} l_1 / h\nu_c$$

photons while running the distance l_2 or l_1.

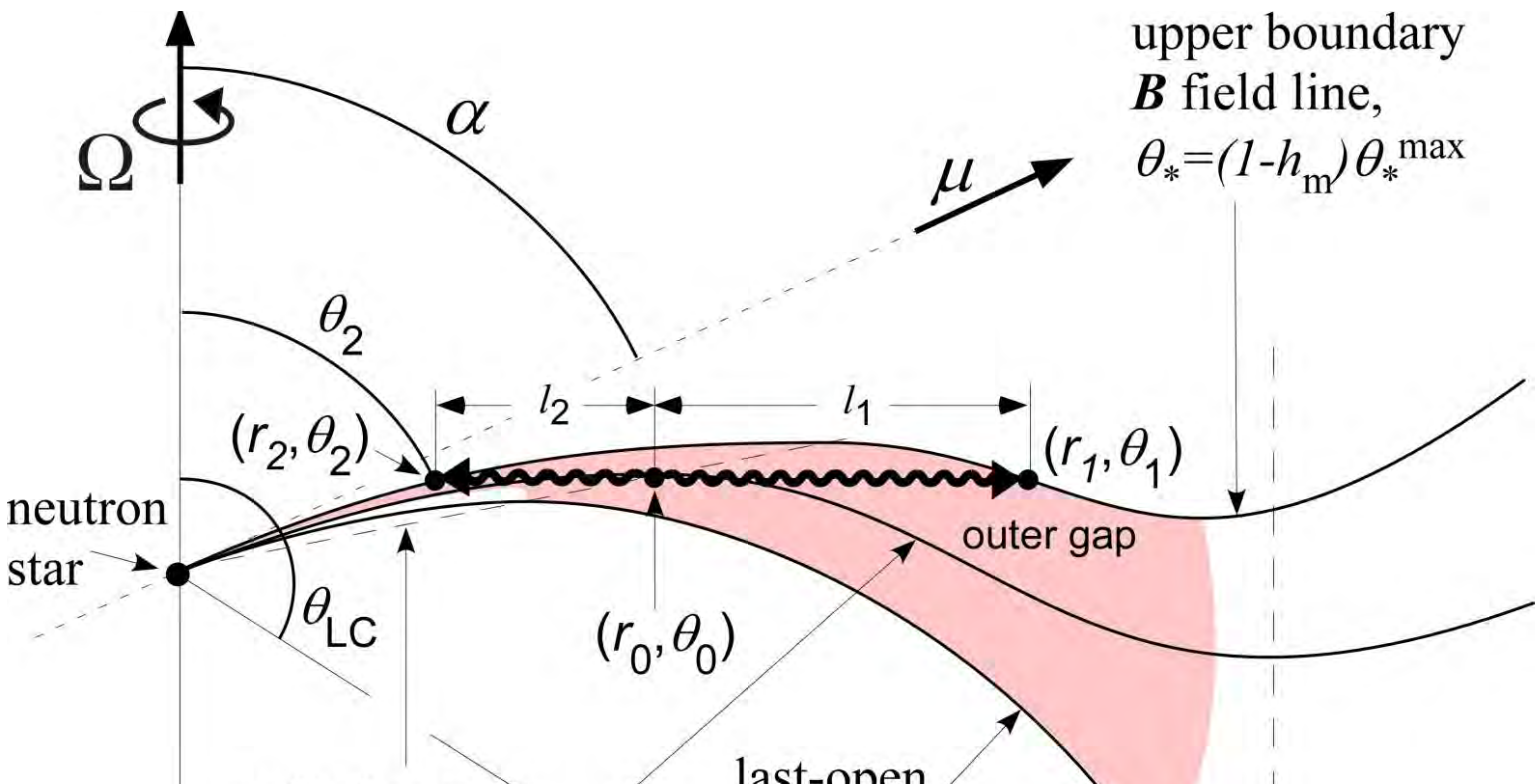

§2 *Analytical derivation of* $L\gamma$ *vs.* L_{spin}

Step 1: express $N_\gamma^{\text{in}}\tau^{\text{in}}$ and $N_\gamma^{\text{out}}\tau^{\text{out}}$ with P,μ,α,T, h_{m}.

An inward e^- or an outward e^+ emits

$$(N_\gamma)^{\text{in}} = eE_{\parallel} l_2 / h\nu_c, \quad (N_\gamma)^{\text{out}} = eE_{\parallel} l_1 / h\nu_c$$

photons while running the distance l_2 or l_1.

Such photons materialize as pairs with probability

$$\tau^{\text{in}} = l_2 F_2 \sigma_2 / c, \quad \tau^{\text{out}} = l_1 F_1 \sigma_1 / c$$

where F_1, F_2 denotes the X-ray flux and σ_1, σ_2 the pair-production cross section.

Quantities l_1, l_2, F_1, F_2, σ_1, σ_2 can be expressed by P,μ,α,T, and h_{m}, if we specify the ***B*** field configuration.

§2 *Analytical derivation of* L_γ *vs.* $L_{\rm spin}$

Step 2: Give spin-down law and NS cooling curve.

Assume dipole-radiation formula,

$$-I\Omega\dot{\Omega} = \frac{2}{3}\frac{\mu^2\Omega^4}{c^3} \quad \rightarrow \; P = P(t, \alpha)$$

Adopt the minimum cooling scenario (i.e., without any direct-Urca, rapid cooling processes).

$$\rightarrow \; T = T(t)$$

§2 Analytical derivation of $L\gamma$ vs. $L_{\rm spin}$

Cooling curves in the minimum cooling scenario:

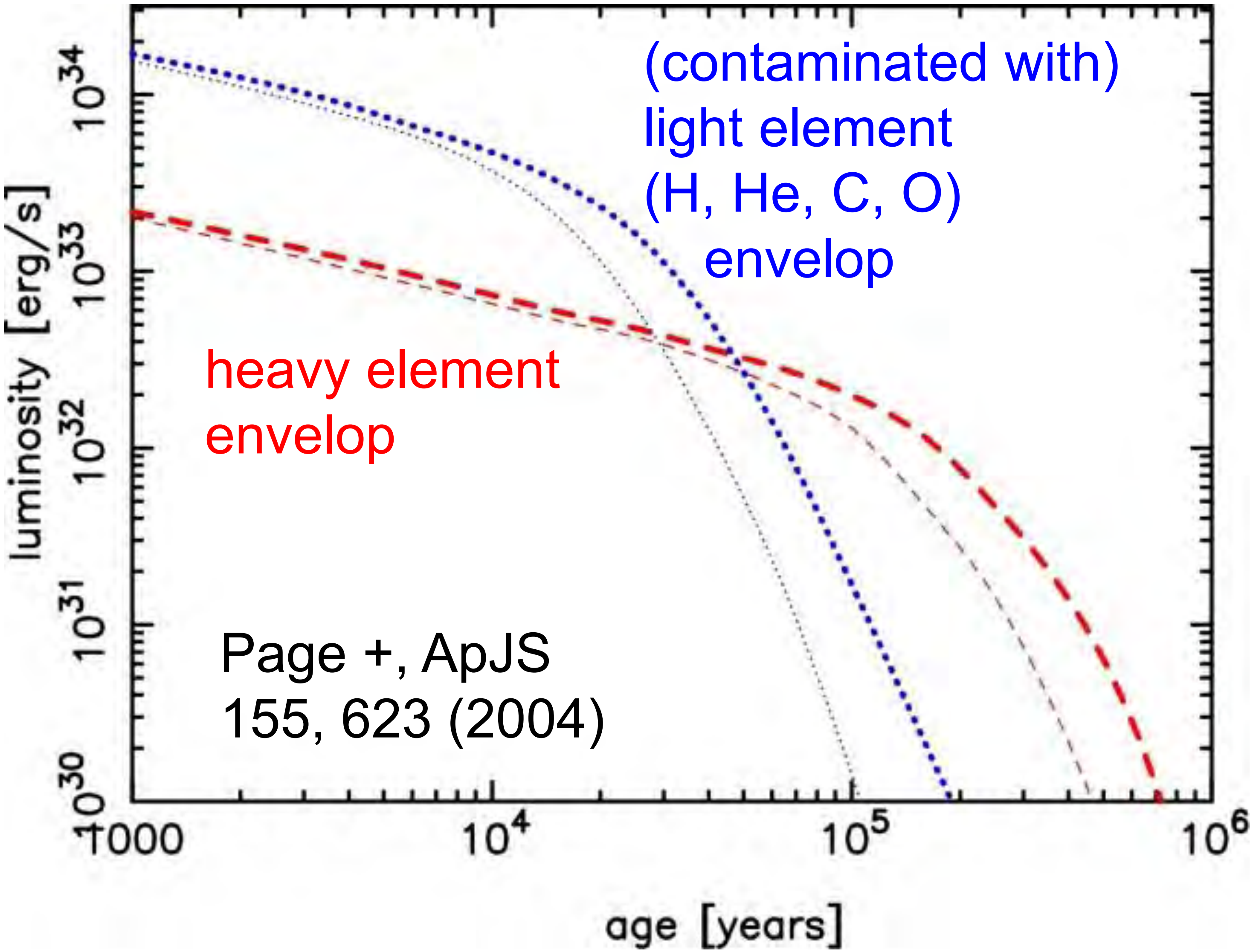

Step 2: Now we can solve $h_m = h_m(t)$.

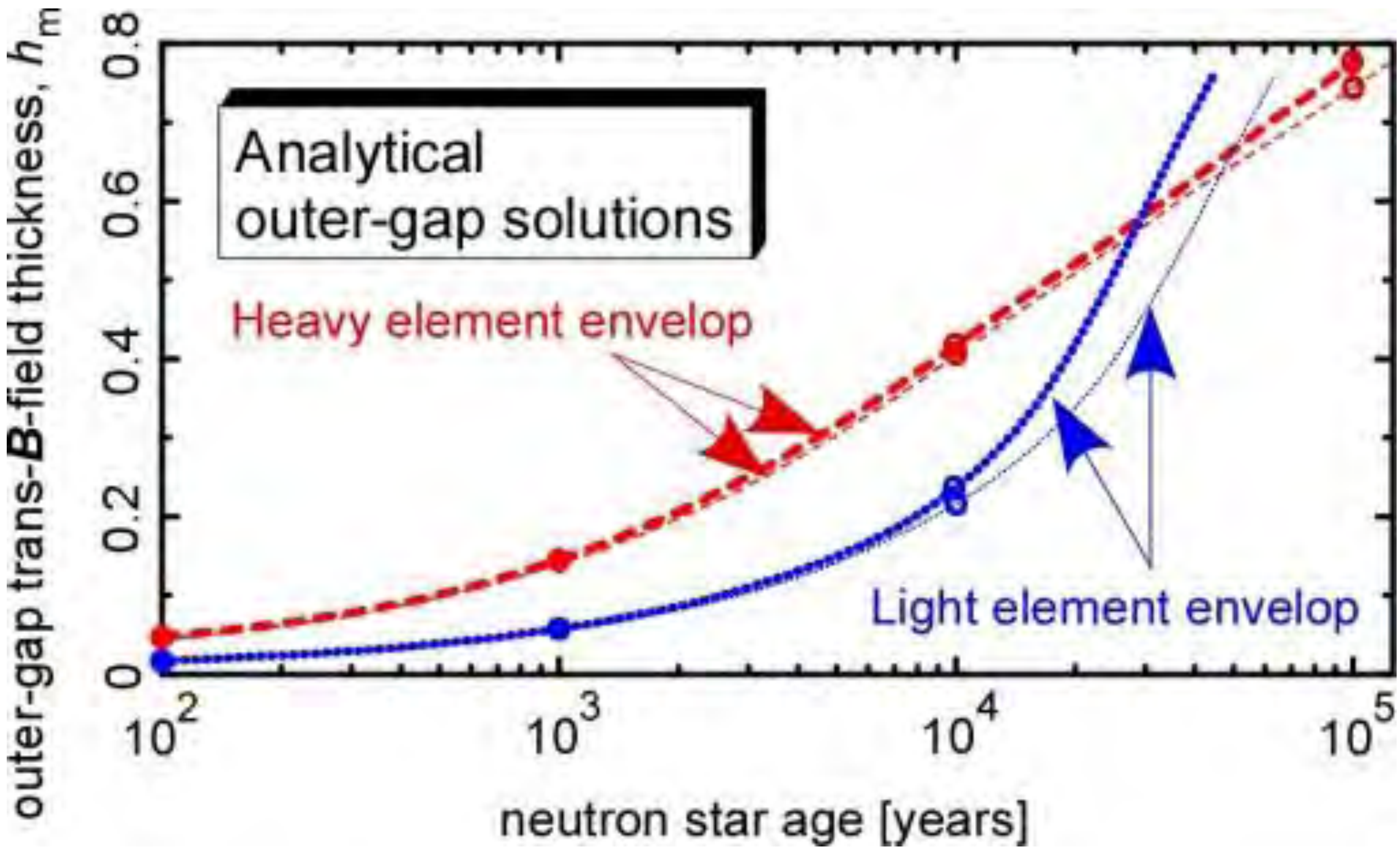

§2 *Analytical derivation of* L_γ *vs.* L_{spin}

Step 3: We can immediately solve $\dot{E} = \dot{E}(t, \alpha)$ by the spin-down law.
Assume α=90°.

(trivial)

§2 *Analytical derivation of* $L\gamma$ *vs.* L_{spin}

Step 4: Use $h_m = h_m(t)$ to relate $L_\gamma \propto h_m{}^3 \dot{E}$ with $\dot{E} = \dot{E}(t)$.

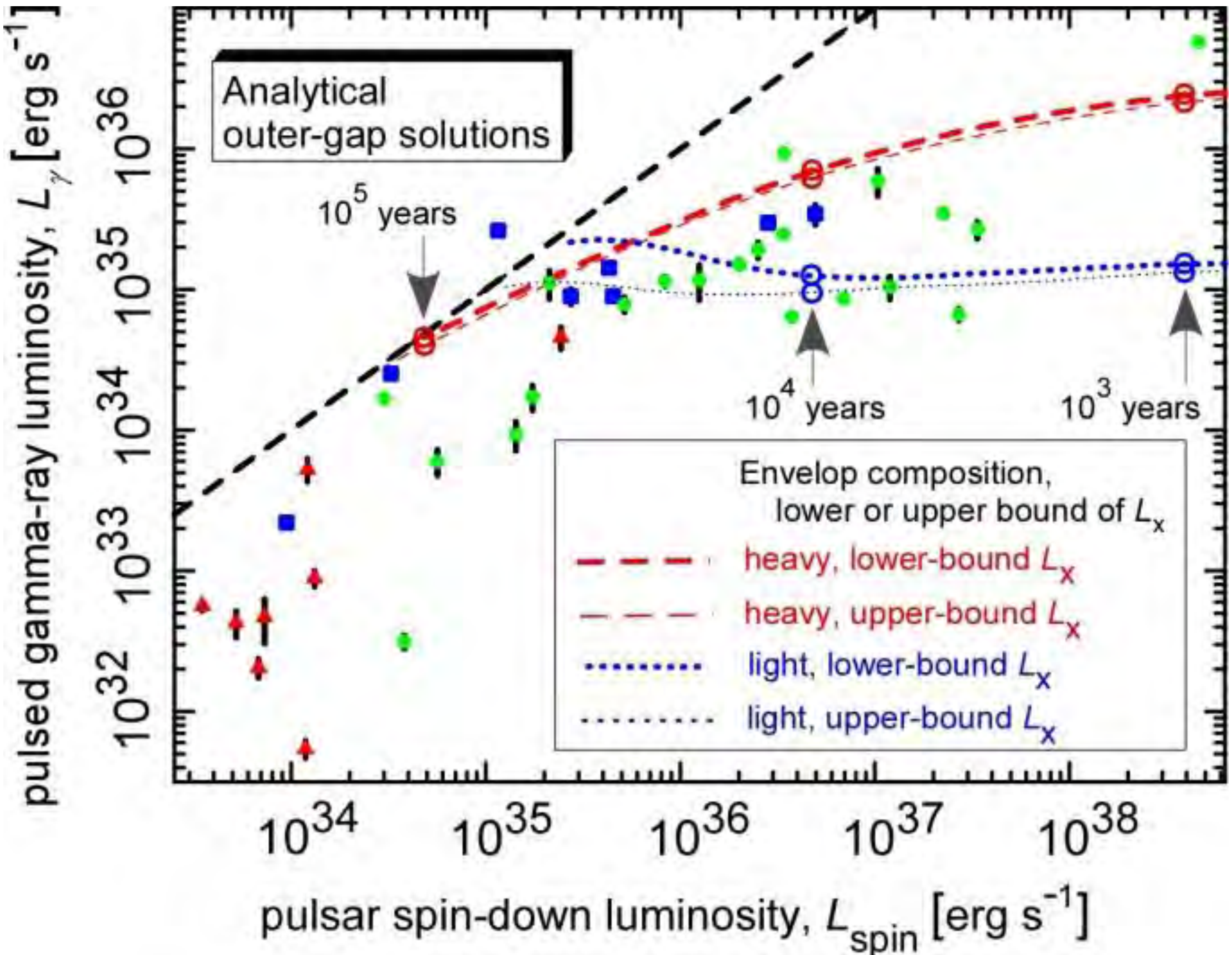

§3 *Numerical derivation of* $L\gamma$ *vs* $L_{\rm spin}$

Second, let us derive the evolution of L_γ numerically.

For this purpose, we simultaneously solve

(1) Poisson eq. for electrostatic potential,
(2) Boltzmann eqs. for electrons/positrons,
(3) Radiative transfer eq. for emitted photons

in the 3-D pulsar magnetosphere under the BDCs,

(a) inner BD= NS surface,
(b) lower BD= last-open ***B*** lines,
(c) outer, upper BD is determined as a free-BD,
(d) No $e^{\pm}$ injection across inner/outer BDs,
(e) No photon injection across inner/outer BDs.

§3 Numerical derivation of $L\gamma$ vs $L_{\rm spin}$

The Poisson equation for the electrostatic potential ψ is given by

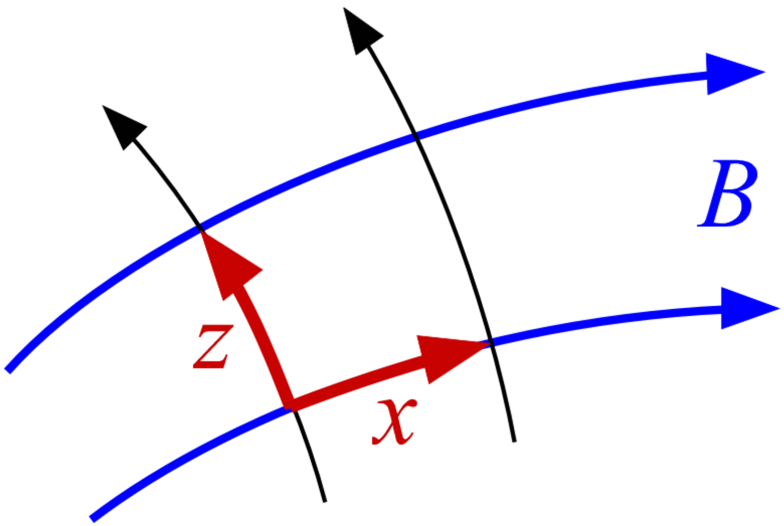

$$-\nabla^2\psi = 4\pi(\rho - \rho_{\rm GJ}) \ ,$$

where

$$E_{\|} \equiv -\frac{\partial\Psi}{\partial x} \ , \ \rho_{\rm GJ} \equiv -\frac{\mathbf{\Omega}\bullet\mathbf{B}}{2\pi c},$$

$$\rho \equiv e\int_0^\infty d\mathbf{p}^3 \left[N_+(\mathbf{x},\mathbf{p}) - N_-(\mathbf{x},\mathbf{p})\right] + \rho_{\rm ion} \ .$$

N_+/N_-: distrib. func. of e^+/e^-

$\boldsymbol{p}$: momentum of e^+/e^-

§3 *Numerical derivation of* $L\gamma$ *vs* L_{spin}

Assuming $\partial_t + \Omega\partial_\phi = 0$, we solve the $e^{\pm}$'s Boltzmann eqs.

$$\frac{\partial N_{\pm}}{\partial t} + \vec{v}\cdot\nabla N_{\pm} + \left(e\vec{E}_{\parallel} + \frac{\vec{v}}{c}\times\vec{B} \right)\cdot\frac{\partial N_{\pm}}{\partial \vec{p}} = S_{IC} + S_{SC} + \int \alpha_\nu d\nu \int \frac{I_\nu}{h\nu} d\omega$$

together with the radiative transfer equation,

$$\frac{dI_\nu}{dl} = -\alpha_\nu I_\nu + j_\nu$$

$N_{\pm}$: positronic/electronic spatial # density,
$E_{\parallel}$: mangnetic-field-aligned electric field,
S_{IC}: ICS re-distribution function, $d\omega$: solid angle element,
I_ν: specific intensity, l : path length along the ray
α_ν: absorption coefficient, j_ν: emission coefficient

§3 Numerical derivation of $L\gamma$ vs. L_{spin}

Numerical solution is consistent with the analytical one.

$L\gamma \sim L_{spin}^{\ 0\text{-}0.4}$
if $L_{spin} > 10^{36}$
erg/s

However,
$L\gamma$ declines
rapidly
if $L_{spin} < 10^{35.5}$
erg/s

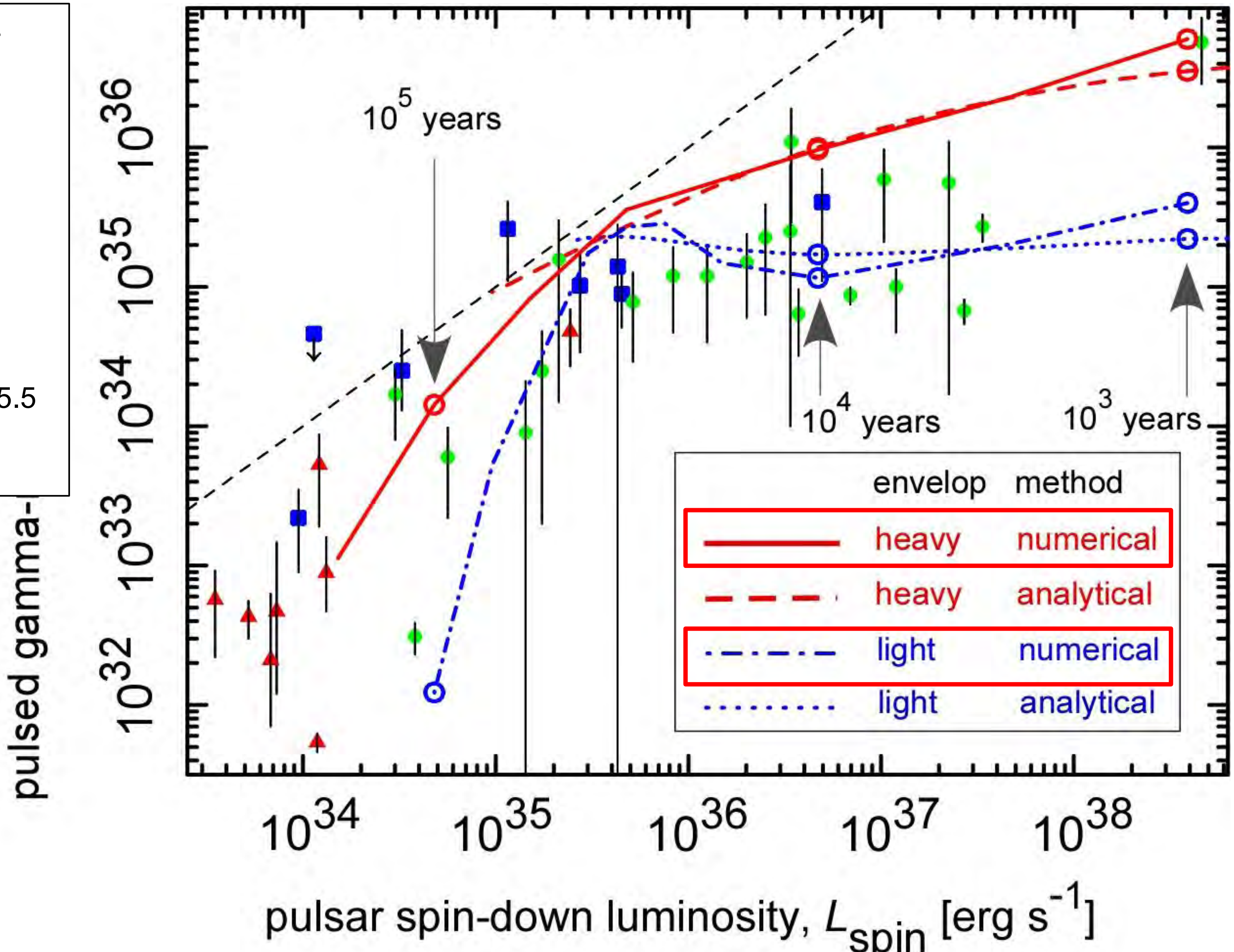

§3 Numerical derivation of $L\gamma$ vs. L_{spin}

Numerical solution is consistent with the analytical one.

For light element envelop, $L\gamma$ peaks around 30 kyrs, as predicted by analytical calculation.

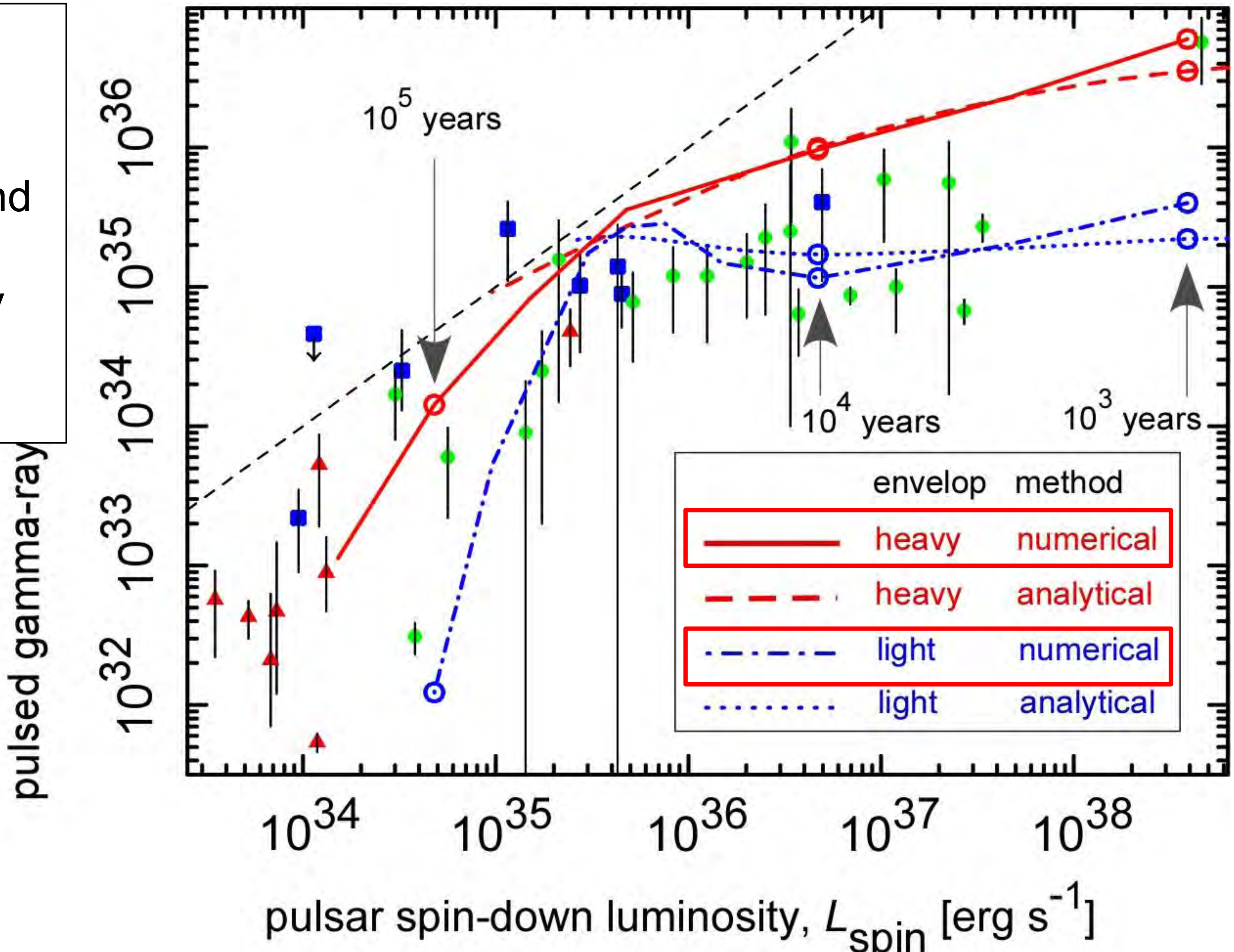

§3 Numerical derivation of Lγ vs. L_{spin}

Numerical solution is consistent with the analytical one.

The actual L_γ will distribute between the two extreme cases.

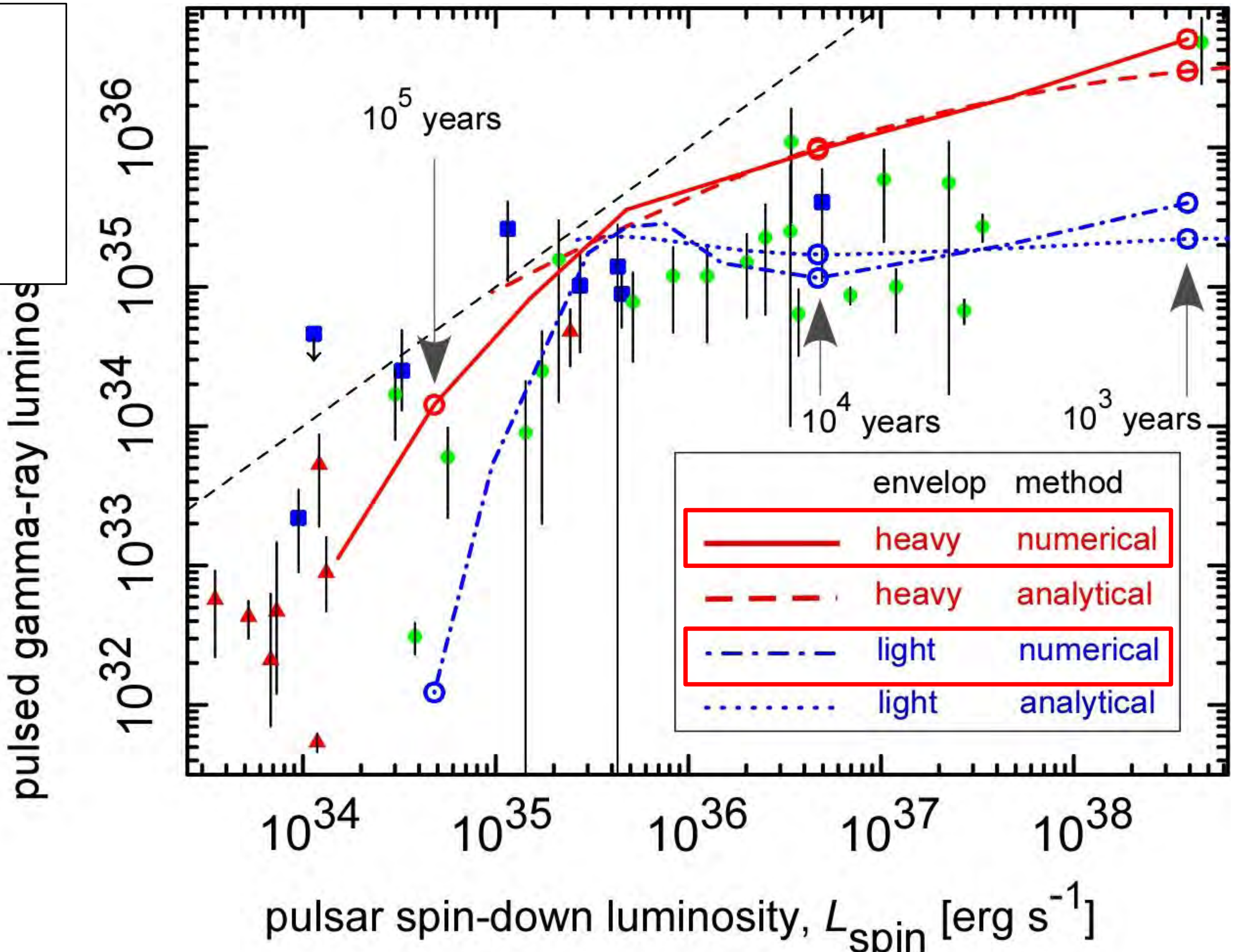

§4 Evolution of exponential cutoff energies

It is worth examining the curvature photon energy, $h\nu_c$.

$h\nu_c$ is regulated below several GeV by self-sustained OG.

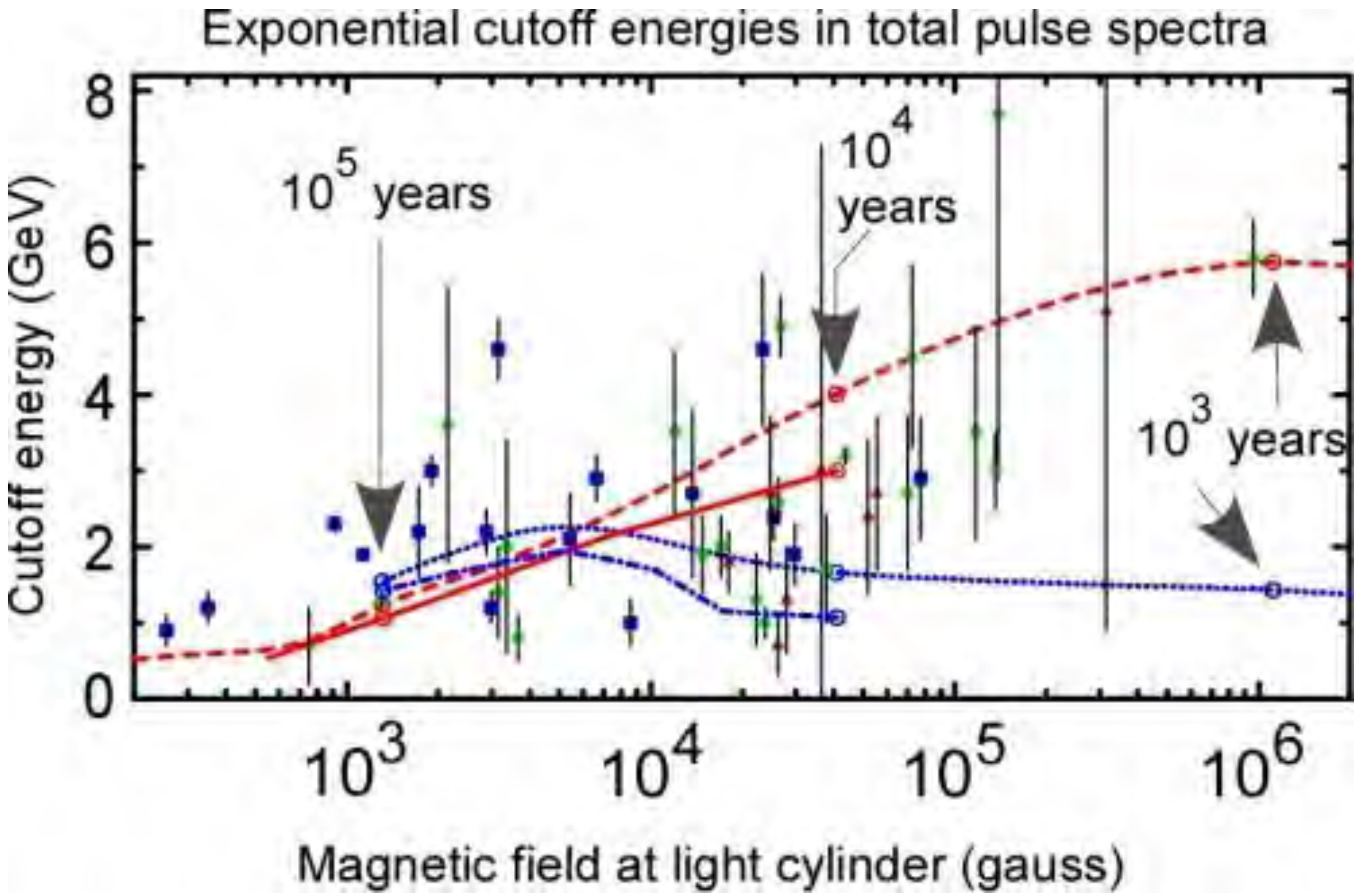

§6 Evolution of gamma-radiation beaming

Finally, take a look at the flux correction factor f_Ω, where $L_\gamma = 4\pi f_\Omega F_\gamma d^2$.

Emission is more beamed along equator as pulsar ages.

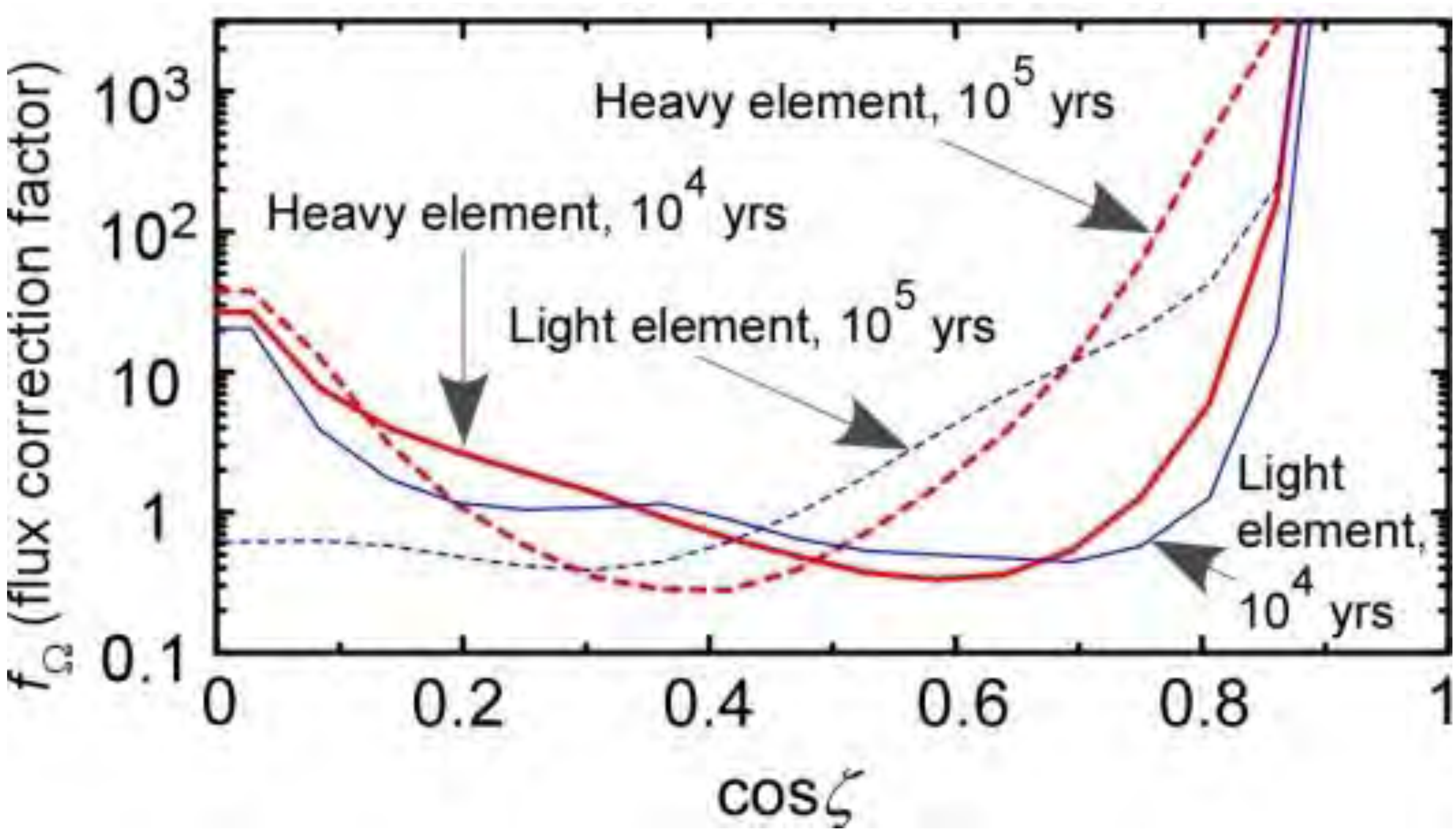

Summary

- We can now solve pulsed high-energy emissions from the set of Maxwell (div$\boldsymbol{E}$=4πρ) and Boltzmann eqs., if we specify P, dP/dt, $\alpha_{\rm incl}$, $kT_{\rm NS}$. We no longer have to assume the gap geometry, $E_{||}$, $e^{\pm}$ distribution functions.

- Gamma-ray luminosity evolves as

$$L_\gamma \propto \dot{E}^{0-0.4} \quad \text{when} \quad \dot{E} < 10^{36.5} \text{ erg s}^{-1}$$

However, it declines more rapidly at $\dot{E} > 10^{36.5}$ erg s^{-1}, because created current becomes much less than GJ value.

- Curvature cutoff energy is self-regulated below several GeV, because $h_{\rm m}$ is suppressed by $E_{||}$ screening due to the polarization of produced pairs.

Thank you.

§7 Modern Outer-gap Model

Self-sustained pair-production cascade in a rotating NS magnetosphere:

$e^{\pm}$'s are accelerated by $E_{\|}$

Relativistic e^+/e^- emit γ-rays via synchro-curvature, and IC processes

γ-rays collide with soft photons/B to materialize as pairs in the accelerator

§8 ICS spectrum of the Crab pulsar

OG can be solved for arbitrary pulsar parameters.

Maxwell & Boltzmann eqs., ⇒

- OG 3-D geometry,
- $E_{||}$ distribution,
- e^+/e^- distribution functions,
- photon specific intensity

Apply this method to the Crab pulsar, assuming

μ=3.8 × 10^{30} G cm^3, α=60^o , kT= 100 eV.

§8 ICS spectrum of the Crab pulsar

3-D distribution of the particle accelerator (i.e., high-energy emission zone) solved from the Poisson eq.:

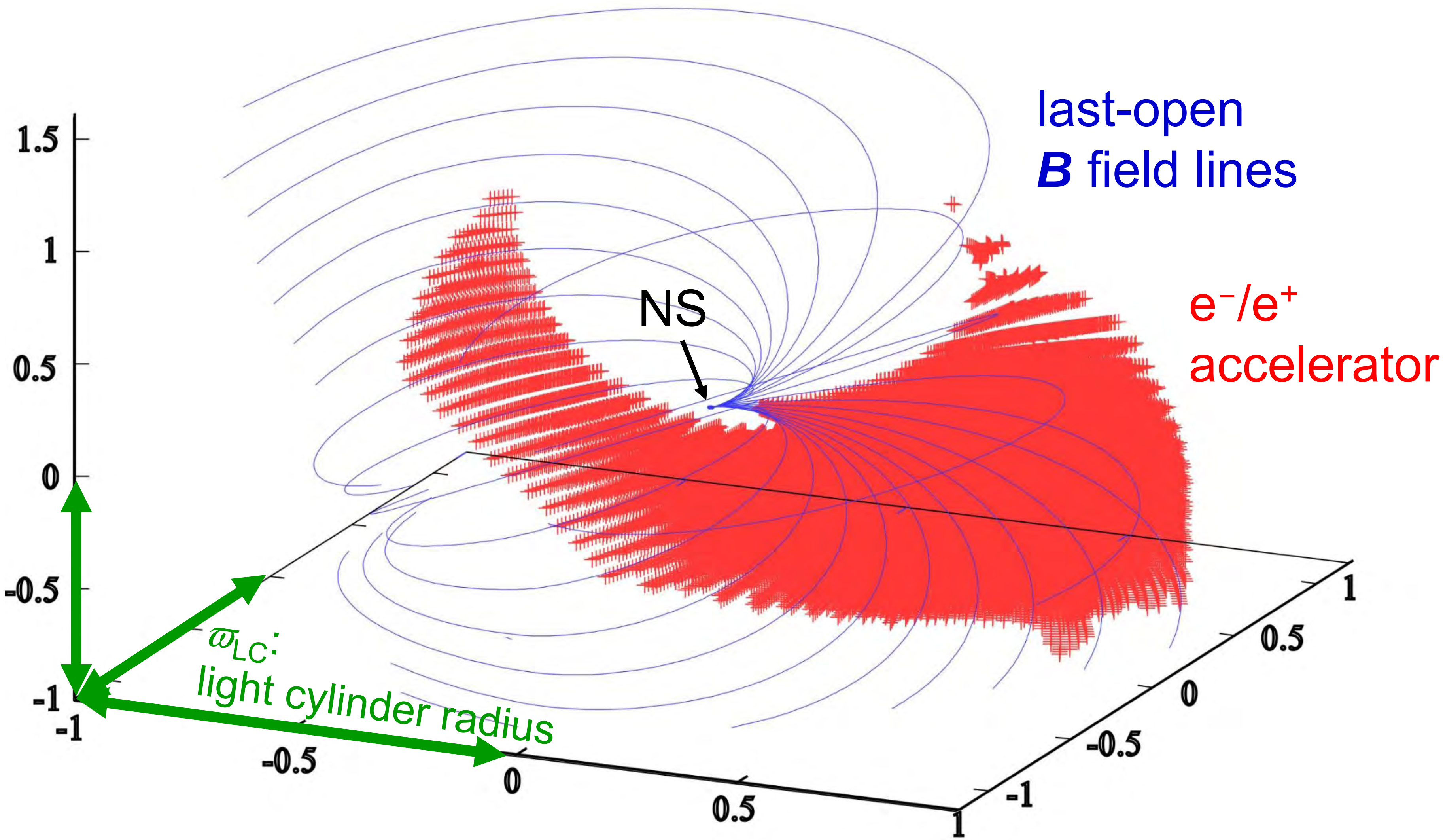

3-D geometry: Trans-field gap thickness is self-regulated by pair production.

Crab, α=60°

Fractional gap thickness projection on the last-open ***B*** line surface

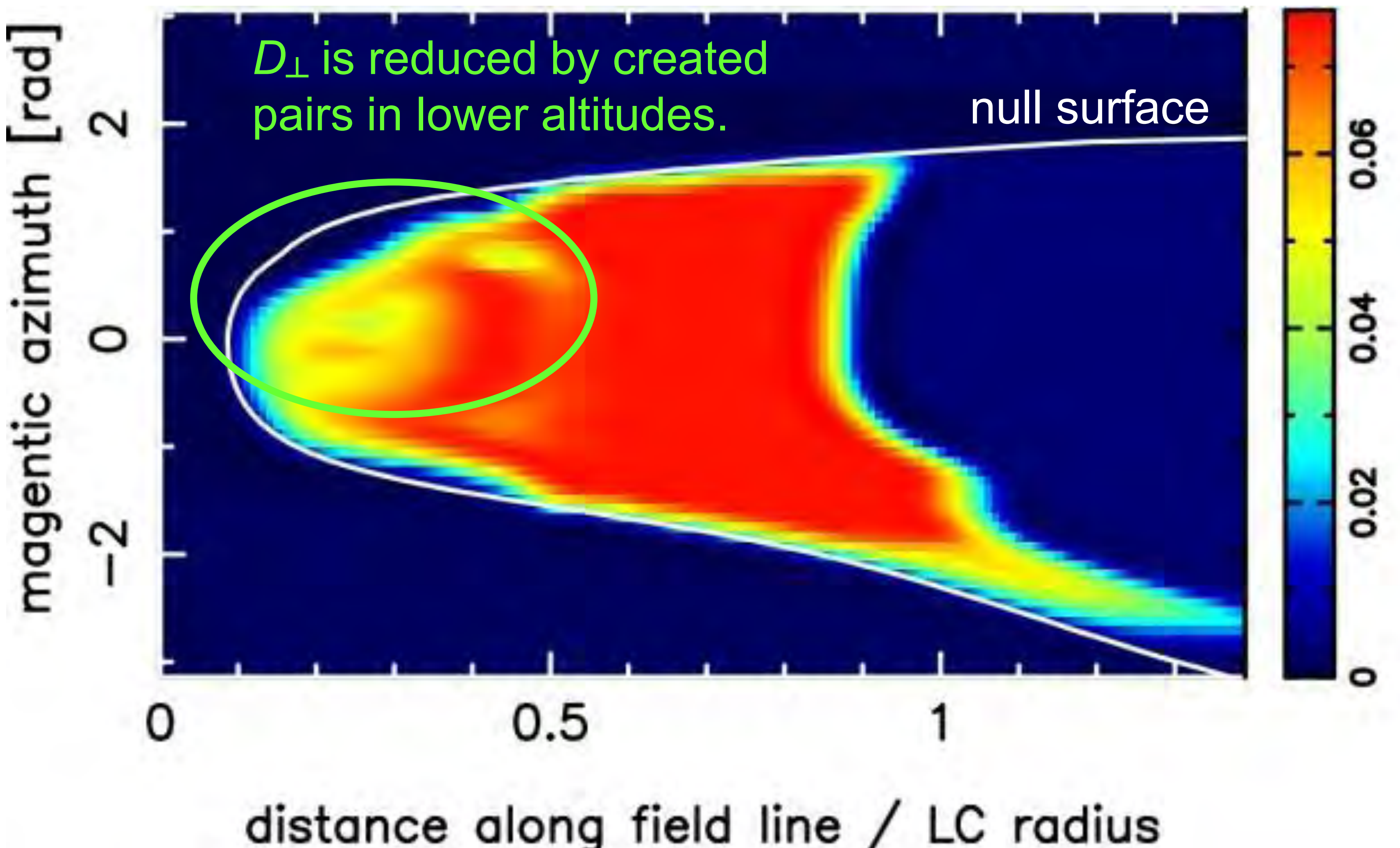

$E_{\parallel}$ is also self-regulated by pair production.

(→ Curvature photon energy changes little for various pulsars.)

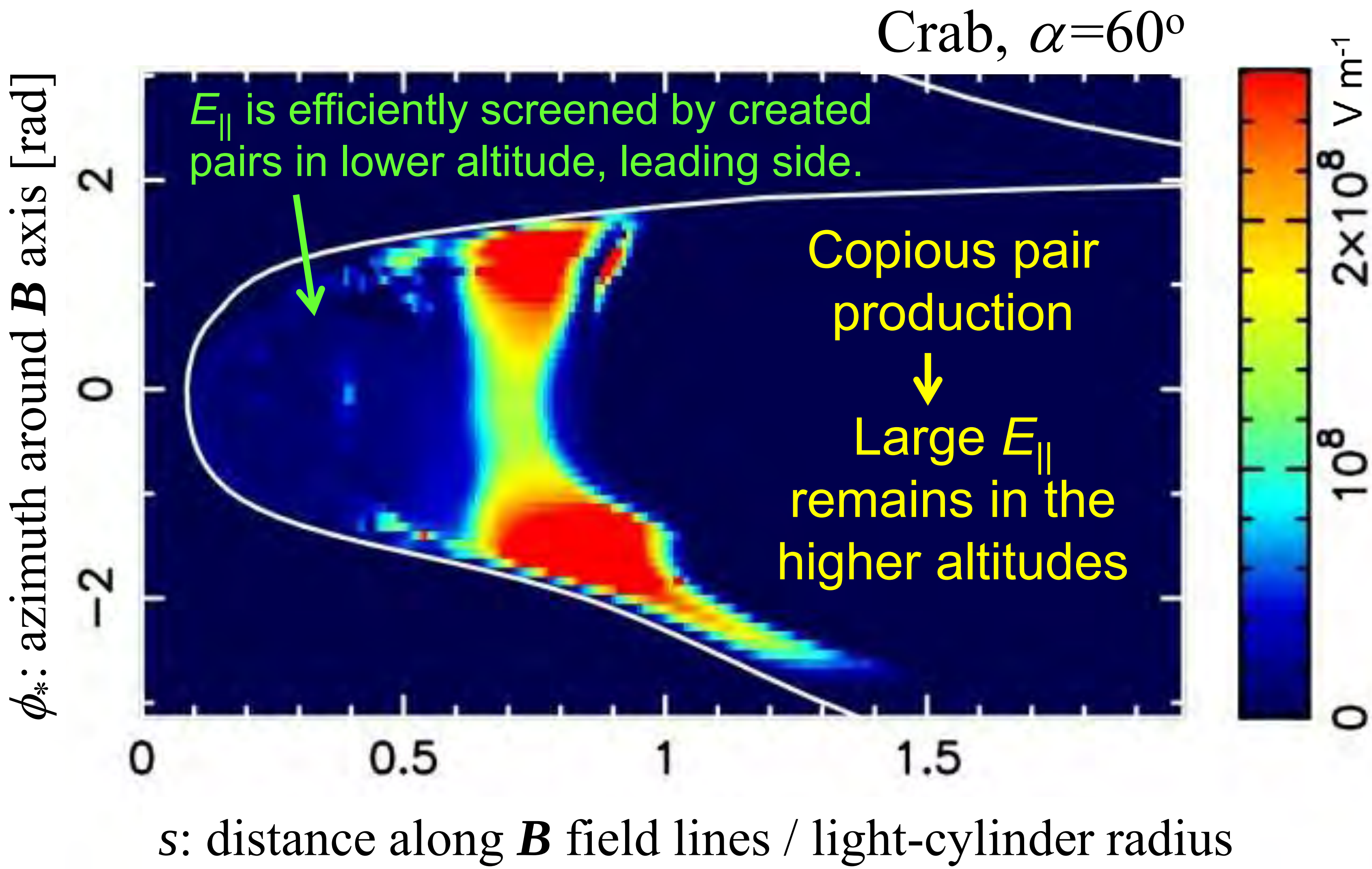

$E_{\parallel}$ is also self-regulated by pair production.

(→ Curvature photon energy changes little for various pulsars.)

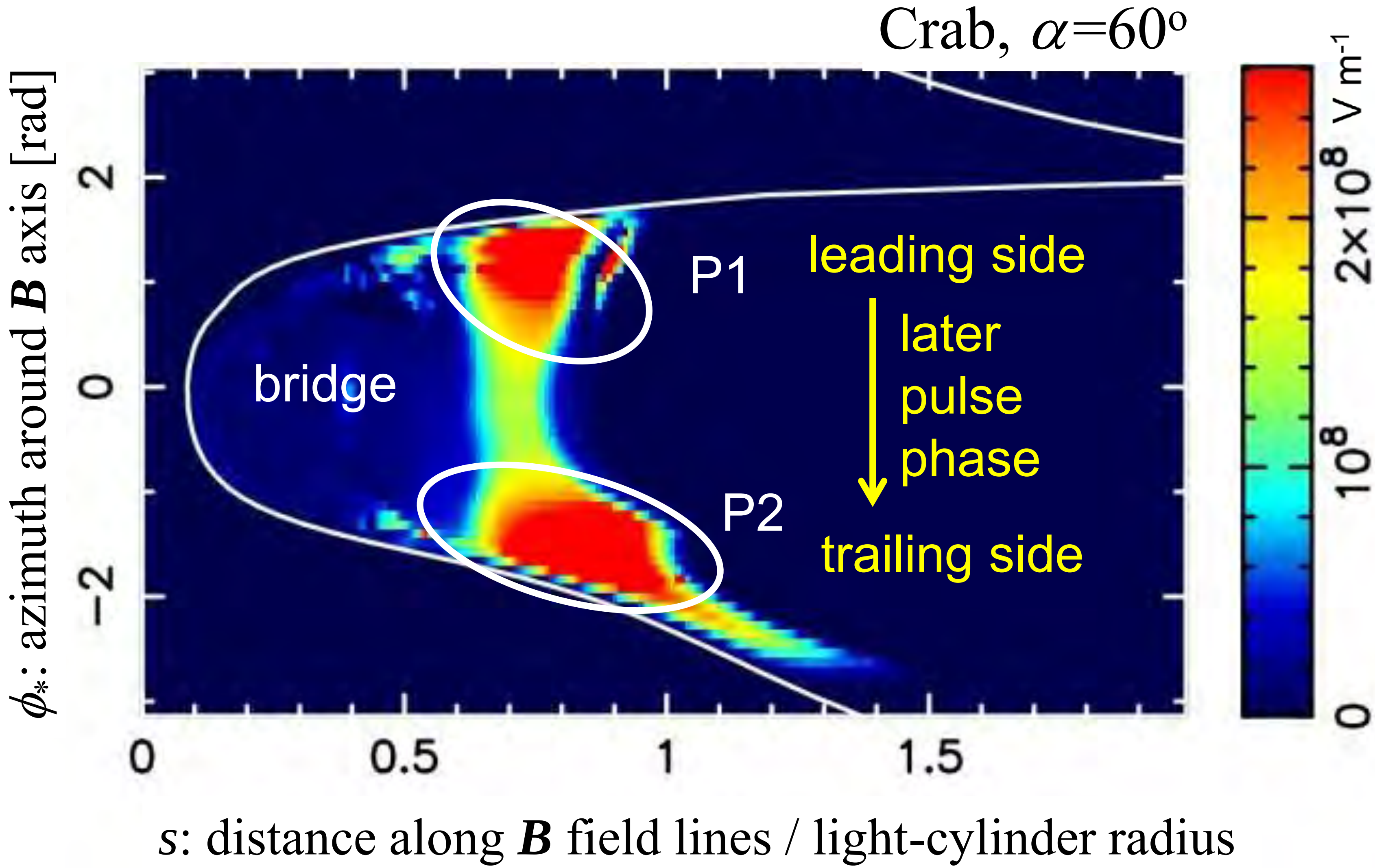

§8 HE/VHE Pulsation from the Crab Pulsar

Crab 60^o

Using $E_{||}$, compute emissivity at each position.

Intensity distribution shows caustic pattern in the sky map.

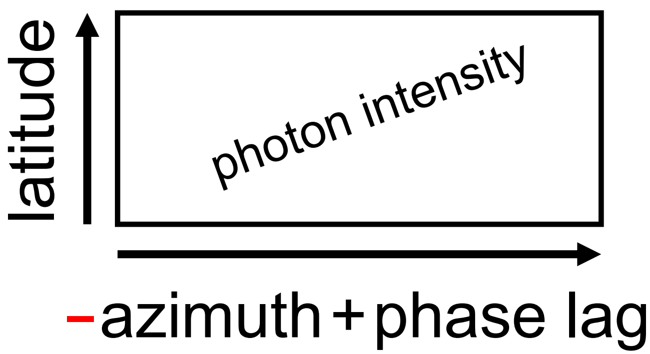

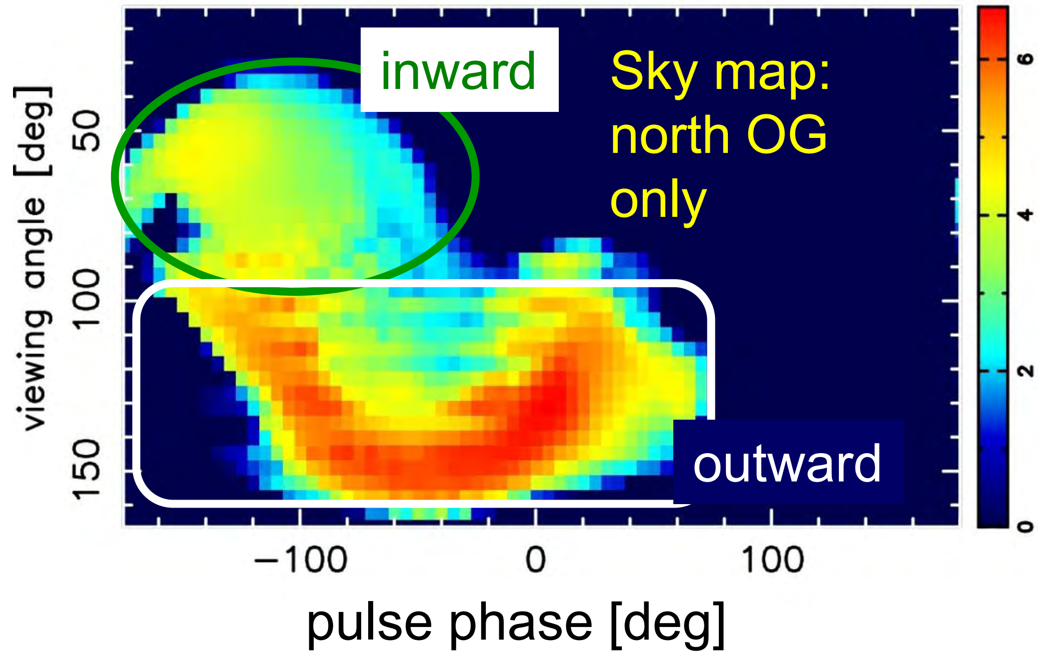

one NS rotation

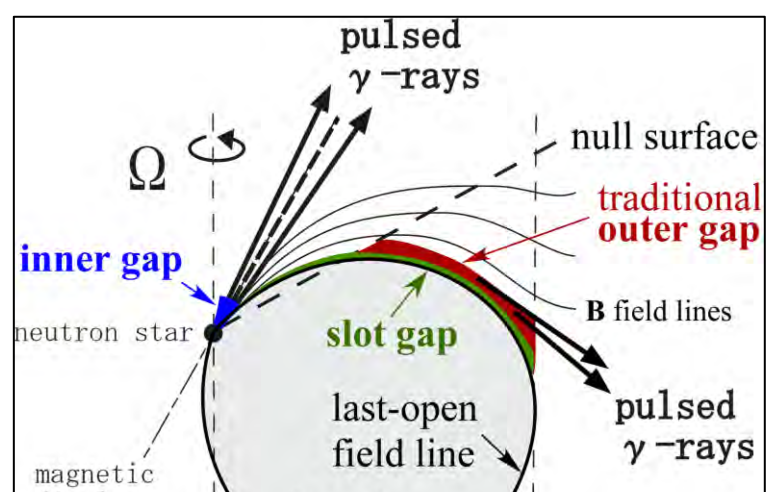

§8 HE/VHE Pulsation from the Crab Pulsar

Crab 60^o

Using $E_{||}$, compute emissivity at each position.

Intensity distribution shows caustic pattern in the sky map.

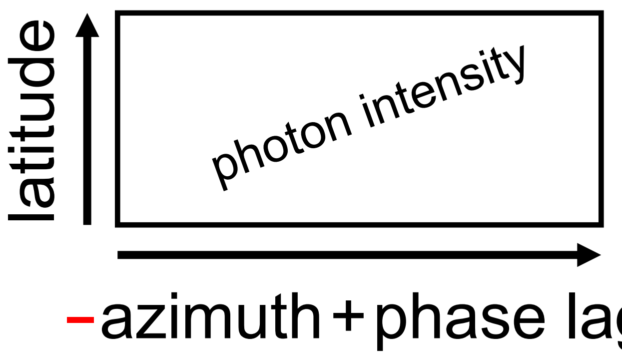

Consider photons emitted from OGs connected to **both poles**.

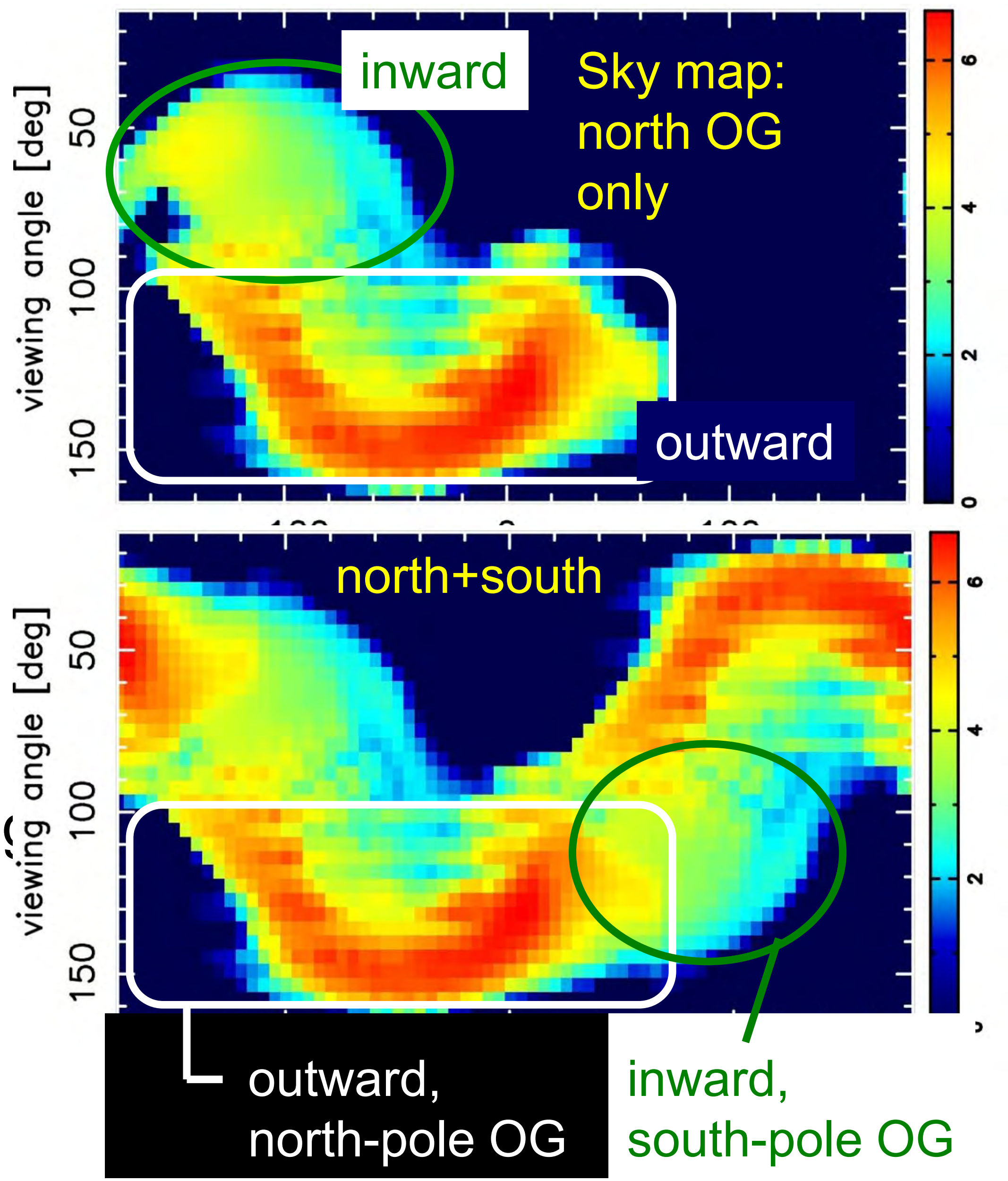

§8 HE/VHE Pulsation from the Crab Pulsar

Crab 60°

Cut the sky map at a viewing angle ζ to obtain a pulse profile.

With energy-dependent sky map, we obtain pulse profiles at different energies.

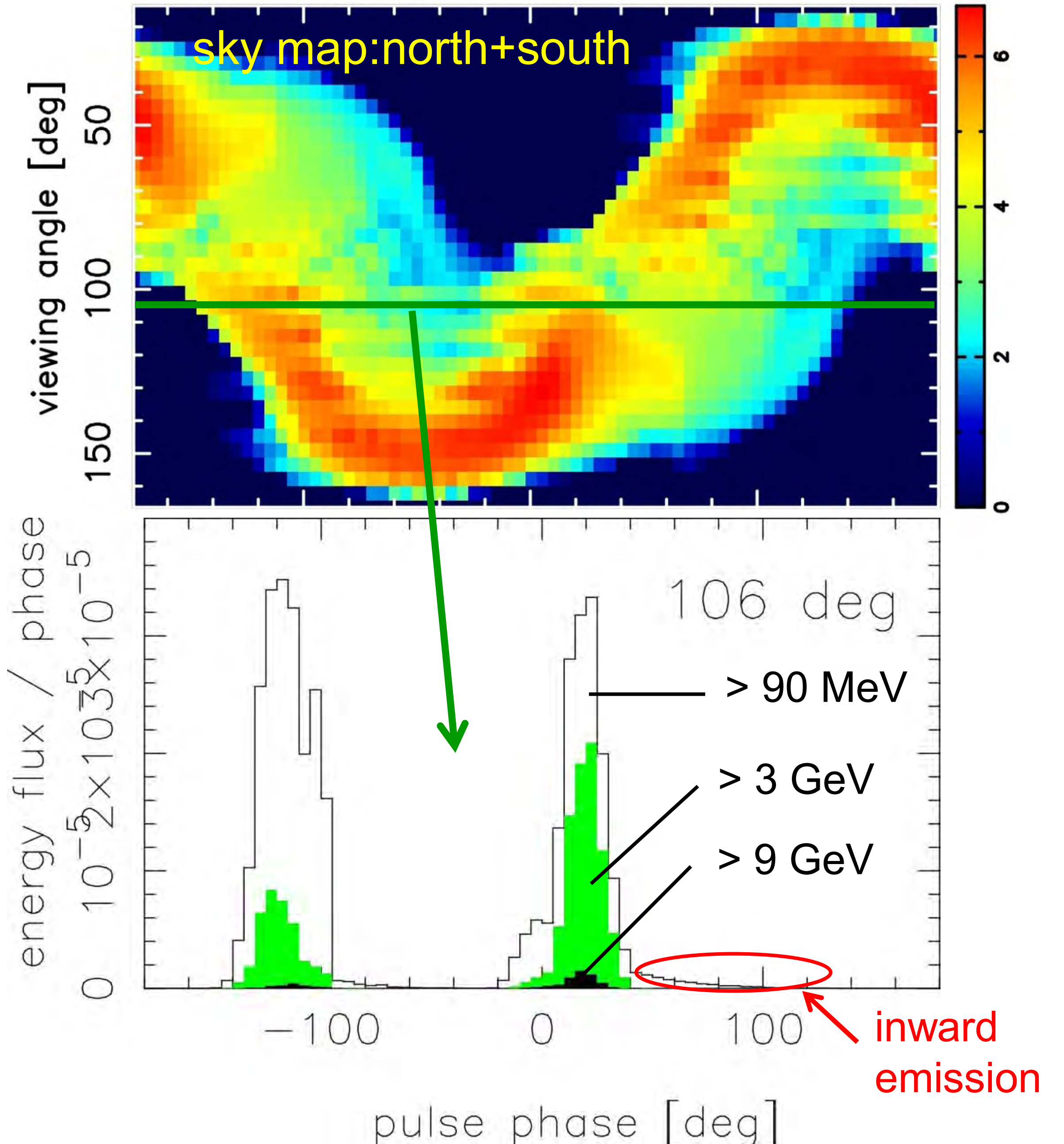

§8 HE/VHE

If we look at the details, however, the energy-dependent pulse profile does not reproduce the Fermi and MAGIC observations.

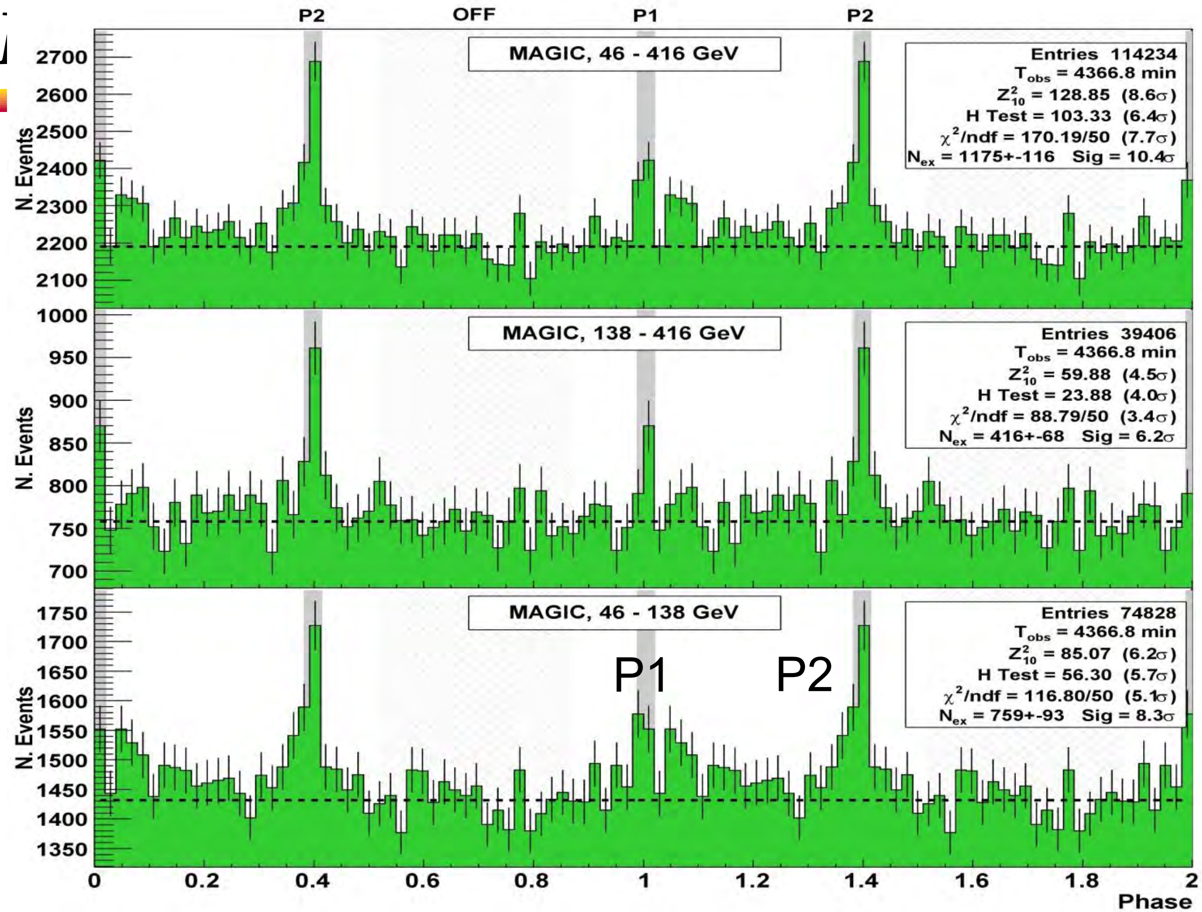

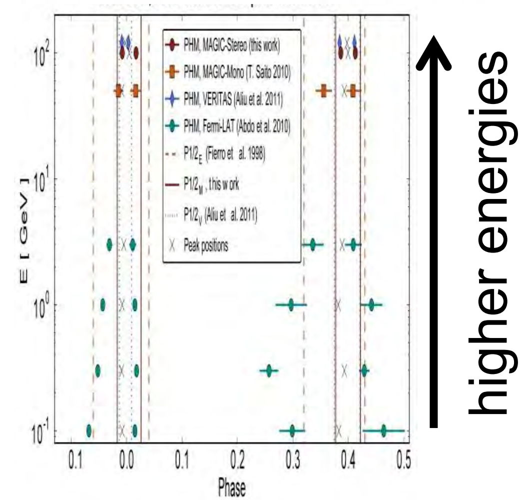

§8 HE/VHE Pulsation from the Crab Pulsar

Some details …

The peak width appears to be roughly constant from 0.1 to 10 GeV, while observed peak width sharpens in higher energies.

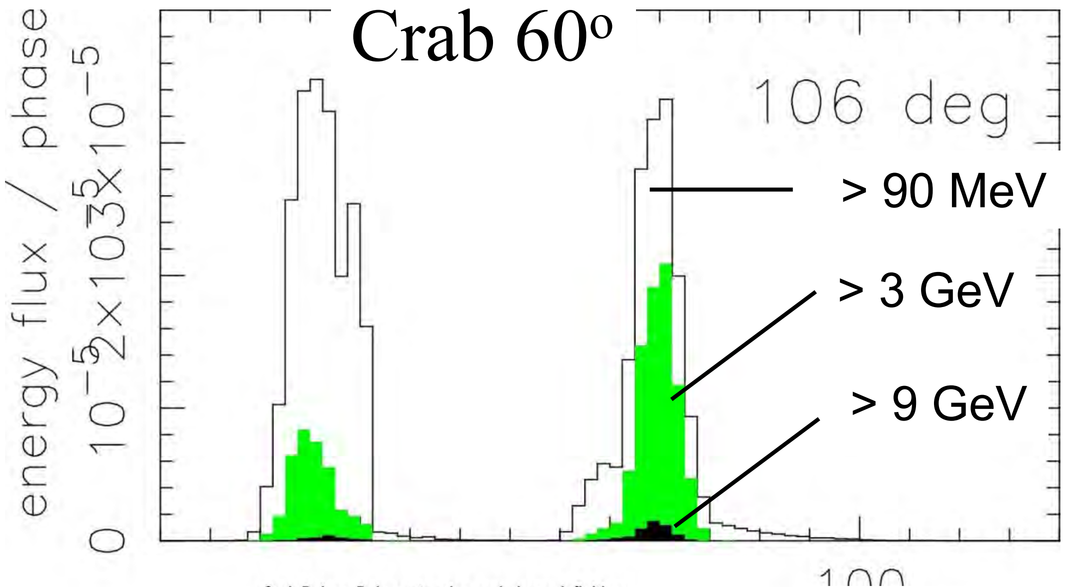

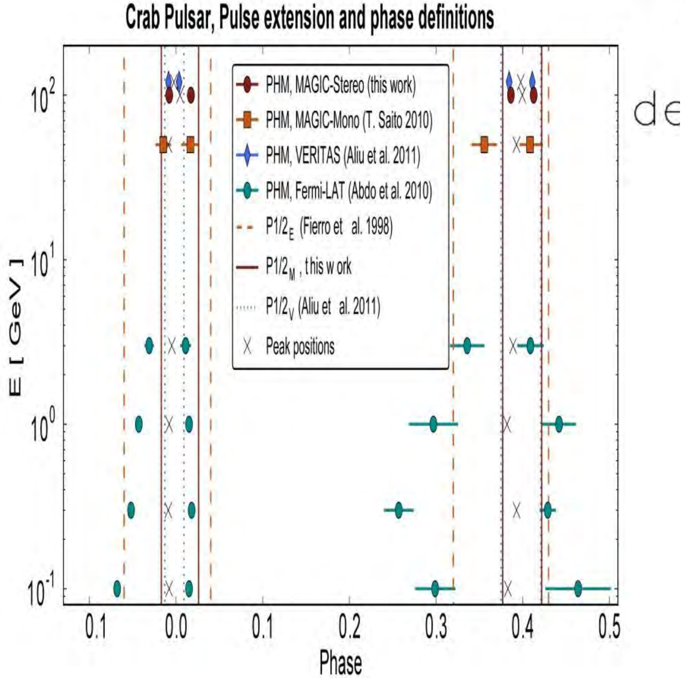

§8 HE/VHE Pulsation from the Crab Pulsar

Phase-averaged spectrum

solid: primary (bef. absorption)
dashed: secondary (bef. absorption)
dotted: tertiary (bef. absorption)
green: all (after absorption)

Crab, α=60°

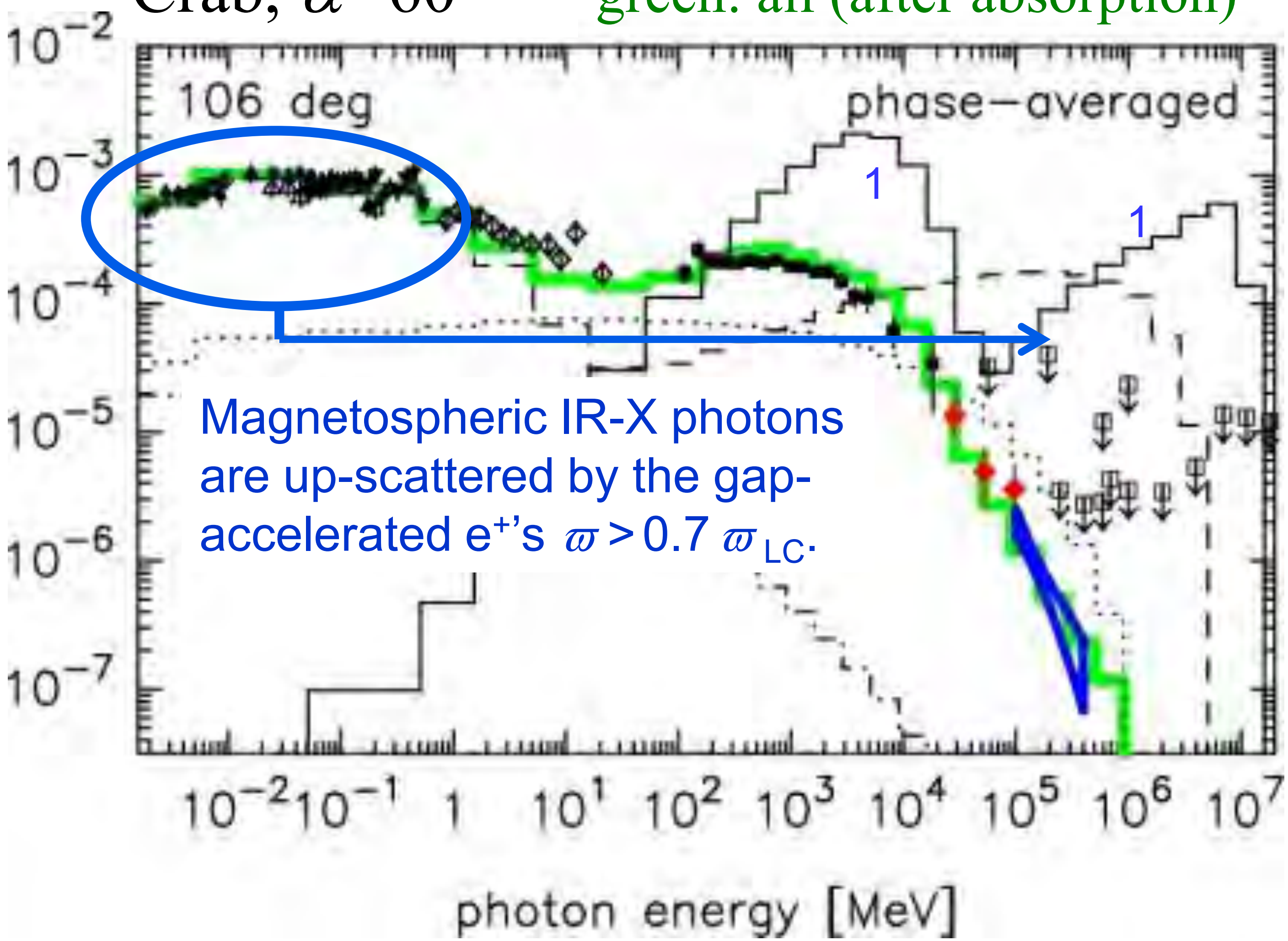

Phase-averaged spectrum

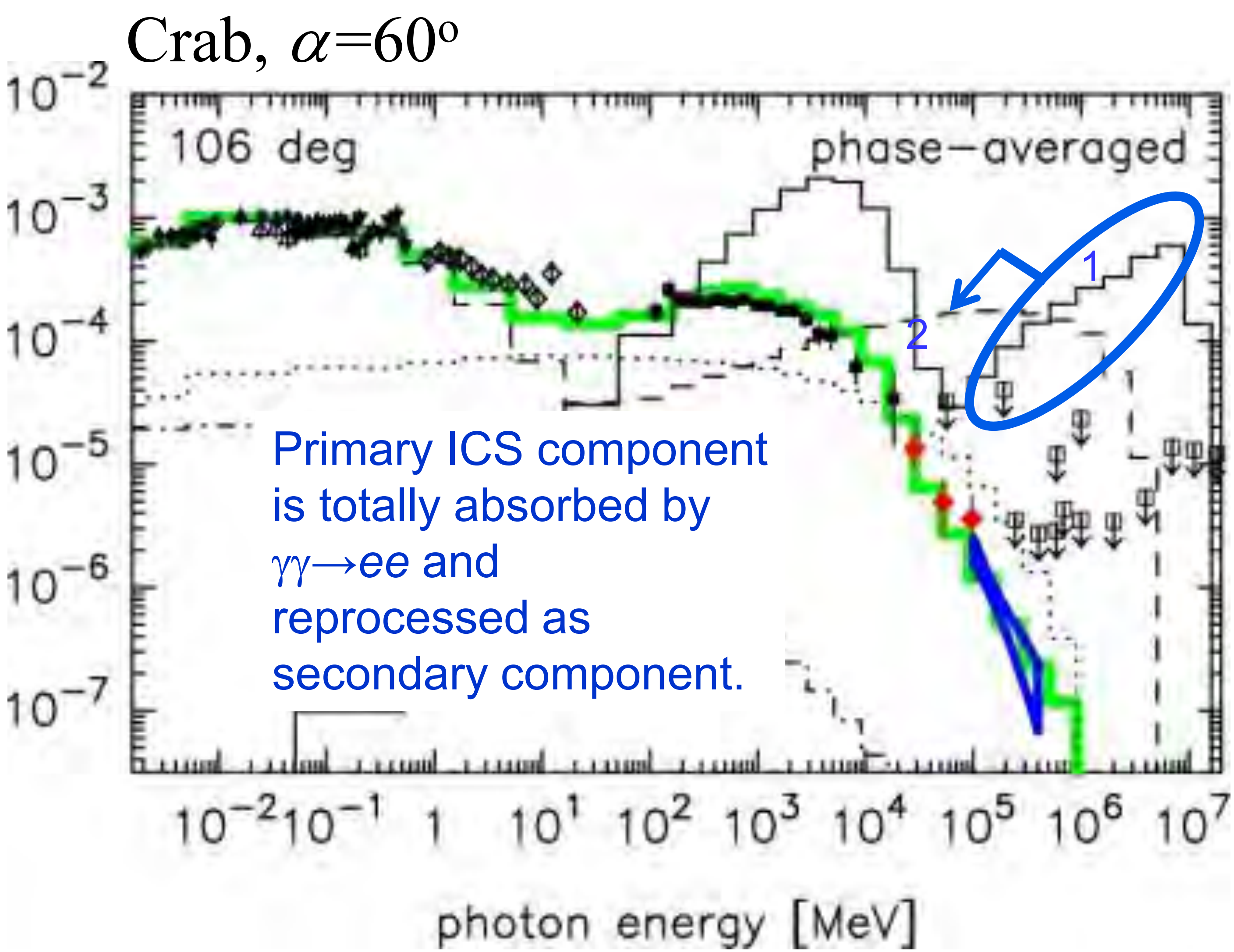

Phase-averaged spectrum

Crab, α=60°

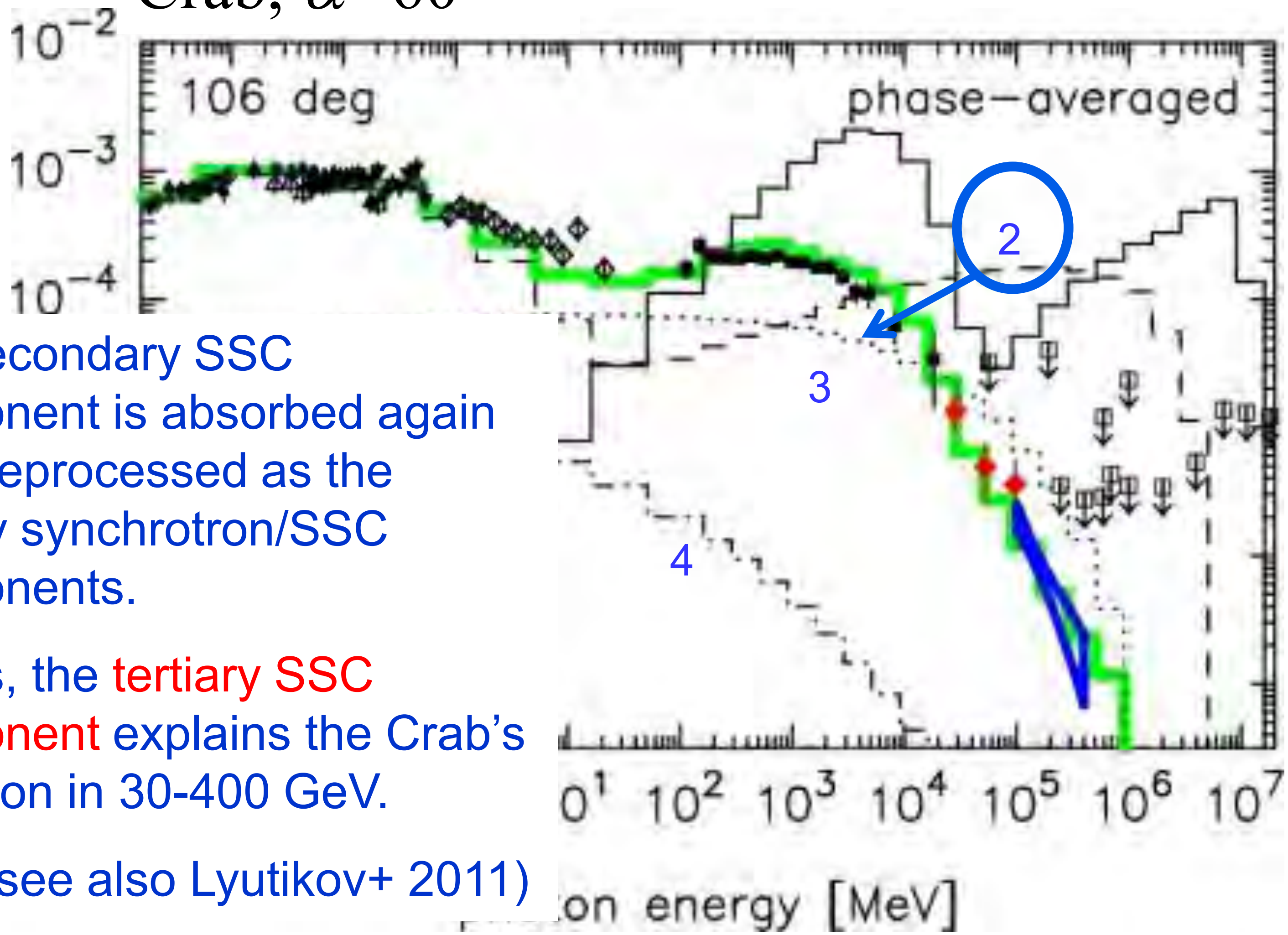

The secondary SSC component is absorbed again to be reprocessed as the tertiary synchrotron/SSC components.

That is, the tertiary SSC component explains the Crab's pulsation in 30-400 GeV.

(see also Lyutikov+ 2011)

§8 HE/VHE Pulsation from the Crab Pulsar

Phase-resolved spectrum (in LAT-defined phase bins):

Crab, α=60^o

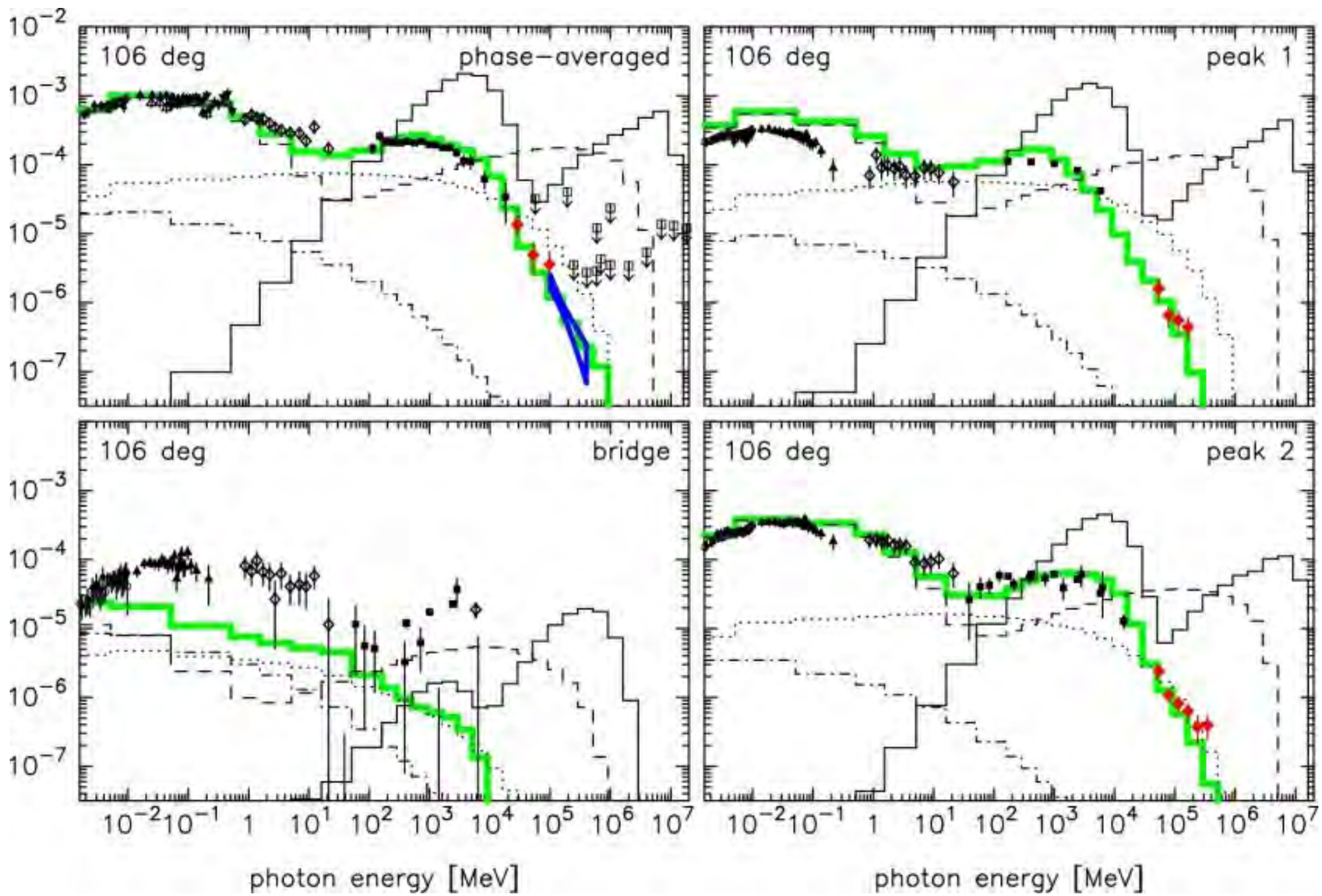

Phase-resolved spectrum (in LAT-defined phase bins):

Crab, α=60°

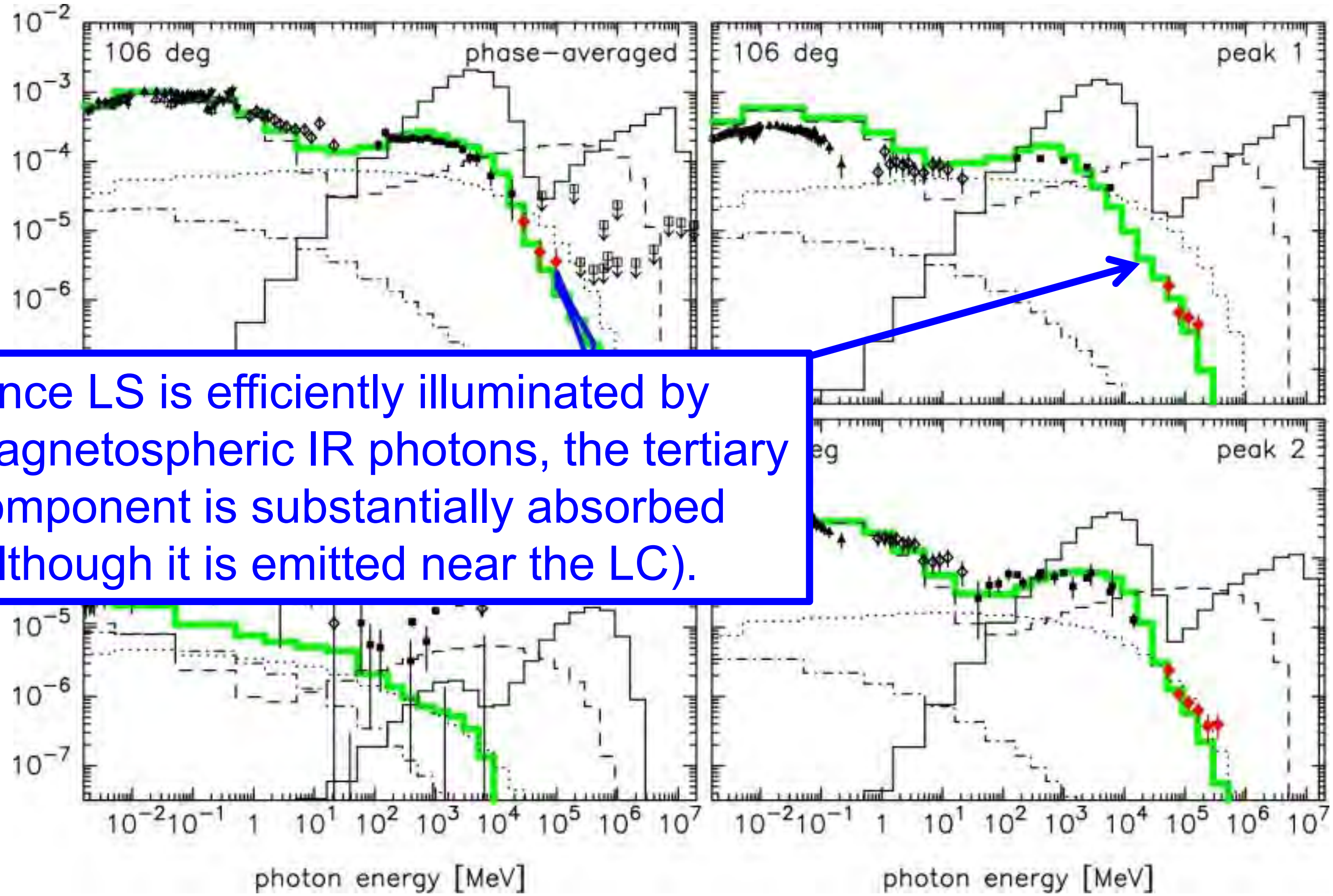

Since LS is efficiently illuminated by magnetospheric IR photons, the tertiary component is substantially absorbed (although it is emitted near the LC).

§8 HE/VHE Pulsation from the Crab Pulsar

Schematic picture of cascading pairs and their emissions:

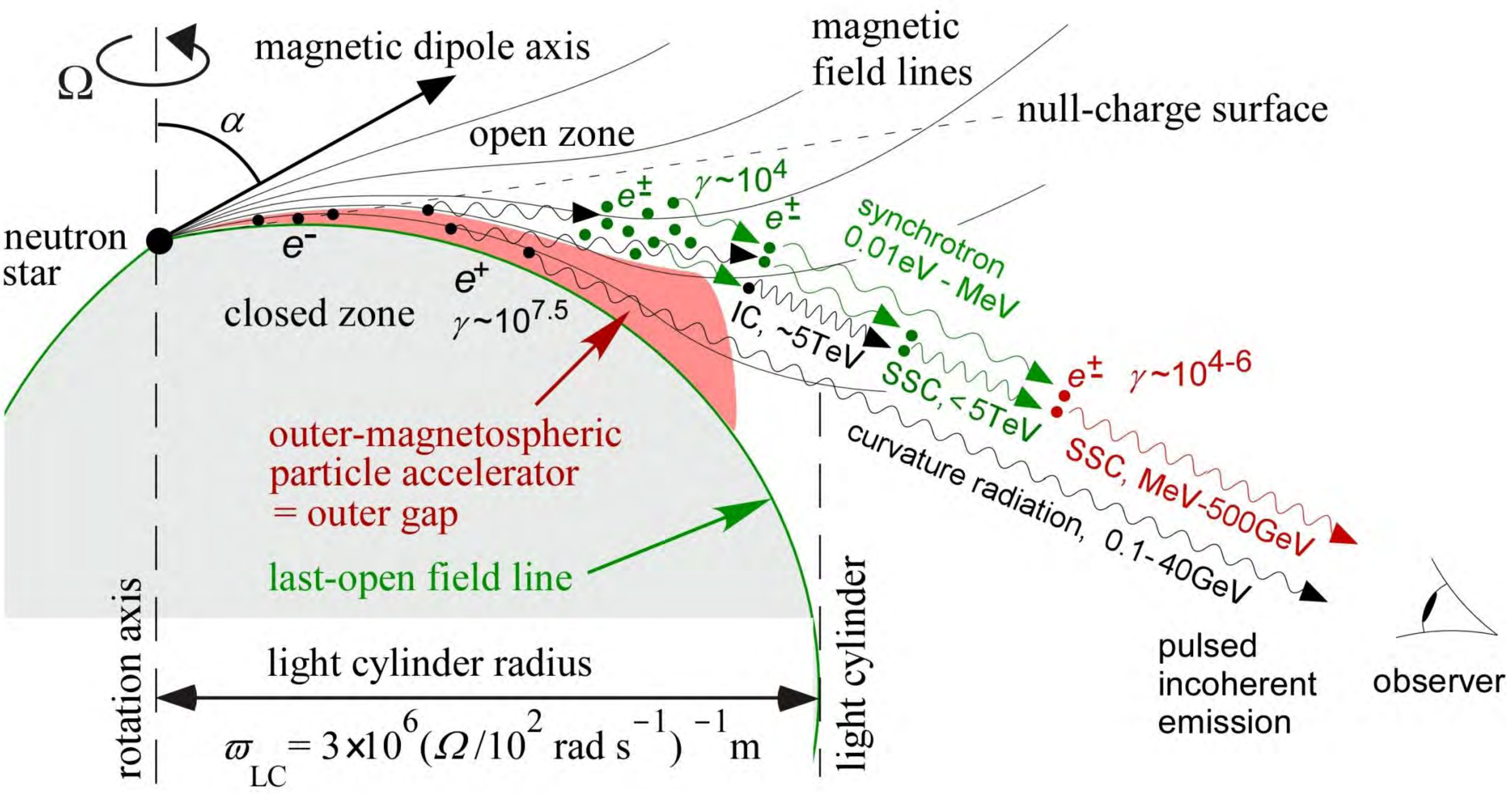

Schematic picture of cascading pairs and their emissions:

Unfortunately, the IC flux is vulnerable to ***B*** geometry near LC.

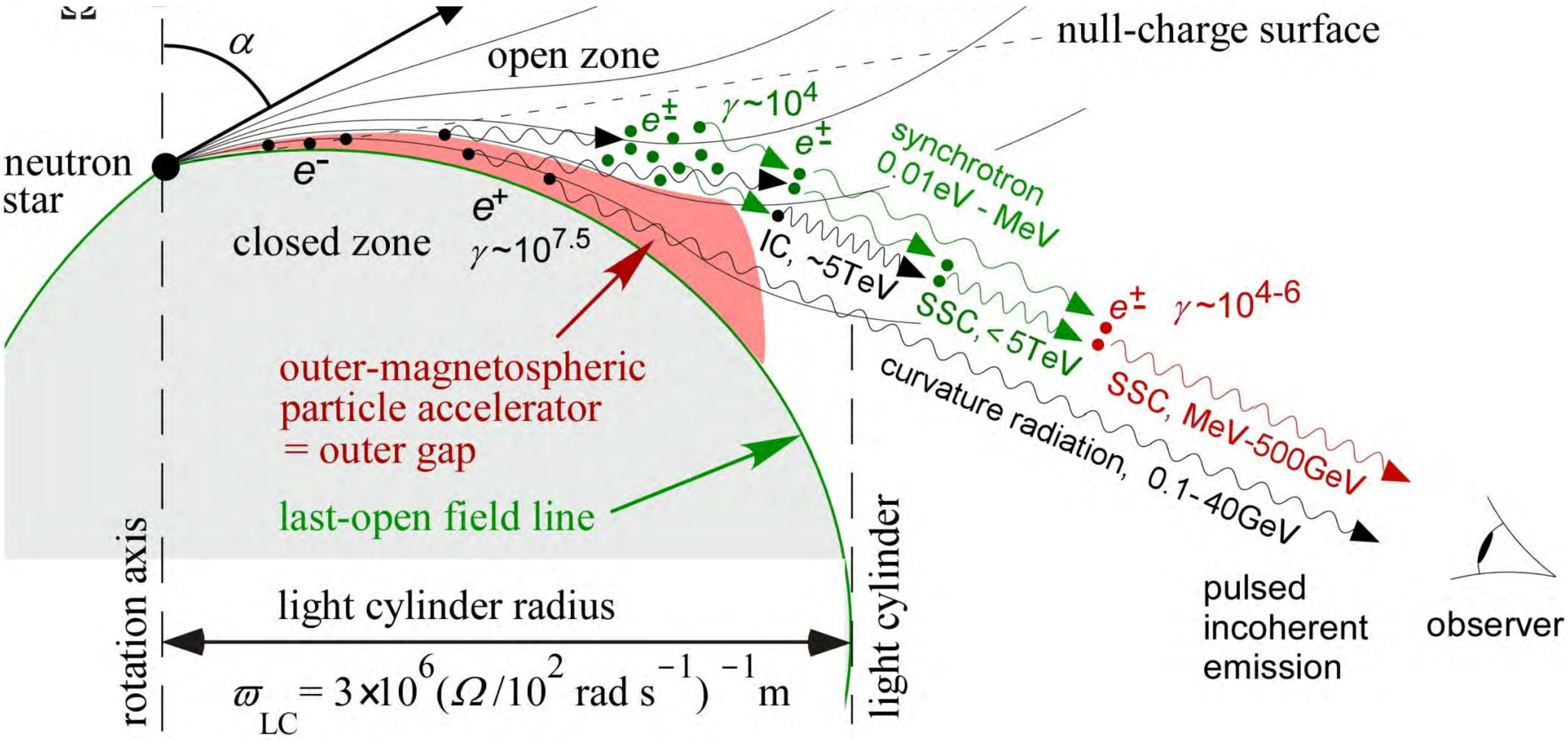

§8 HE/VHE Pulsation from the Crab Pulsar

Schematic picture of cascading pairs and their emissions:

Unfortunately, the IC flux is vulnerable to ***B*** geometry near LC.

Incorporation of correct ***B*** geometry near LC is crucial.